NASA
TP
1869
c.1

TECH LIBRARY KAFB, NM
0067835

NASA Technical Paper 1869

Görtler Vortices and Transition in Wall Boundary Layers of Two Mach 5 Nozzles

Ivan E. Beckwith and Barbara B. Holley

AUGUST 1981

LOAN COPY: RETURN TO
AFWL TECHNICAL LIBRARY
KIRTLAND AFB, N.M.

NASA

TECH LIBRARY KAFB, NM
0067835

NASA Technical Paper 1869

Görtler Vortices and Transition in Wall Boundary Layers of Two Mach 5 Nozzles

Ivan E. Beckwith and Barbara B. Holley
Langley Research Center
Hampton, Virginia

NASA
National Aeronautics
and Space Administration

Scientific and Technical
Information Branch

1981

SUMMARY

The onset of transition in the wall boundary layers of two axisymmetric Mach 5 wind-tunnel nozzles has been measured under conditions of extremely low incident disturbance levels. One nozzle had a rapid expansion contour and a boundary-layer bleed slot just upstream of the throat; the other nozzle was of conventional design. The range of test unit Reynolds numbers, based on conditions at the nozzle exit, was from 6×10^6/m to 2.5×10^7/m.

When the nozzle walls were maintained in a polished and clean condition, transition moved gradually upstream as the test Reynolds number was increased. When transition was some distance downstream of the wall inflection point and in the concave wall region, the values of the local Görtler parameter at transition varied from about 5 to 6, whereas the momentum thickness Reynolds number varied from about 750 to 1050. These results indicated that Görtler vortices were probably involved in the transition process in both nozzles.

Oil flow patterns obtained near the exit of the nozzles indicated that Görtler vortices were always present when the wall boundary layers were laminar. In the rapid-expansion slotted nozzle the vortices persisted far downstream of the transition point when the bleed slot control valves were open. With the bleed valves closed, the wall boundary layer was tripped by the lip of the bleed slot and the vortices were completely obliterated.

Calculations for the growth of Görtler vortices based on new results from linear theory for supersonic flat-plate profiles gave amplification ratios to transition from e^4 to e^{15}. Possible reasons for this wide range in amplification ratios are discussed, but no definite conclusions are yet possible regarding the values of n in a simple e^n type theory for the assumed linear amplification of Görtler vortices to transition in supersonic nozzles.

INTRODUCTION

Noise radiated into the test section of supersonic wind tunnels by turbulent boundary layers on the nozzle walls dominates transition on simple test models (refs. 1 to 6). Test results in a small Mach 5 nozzle (ref. 7) showed that test-section noise levels, expressed as normalized rms pressure fluctuations, were reduced by at least an order of magnitude when the nozzle-wall boundary layer was laminar rather than turbulent. Transition data on a sharp tip cone tested in this nozzle are available (some of these data were published in ref. 8); however, sufficiently high length Reynolds numbers to get transition on the model could not be obtained when the nozzle boundary layer was still laminar over any significant portion of the "acoustic origin" (ref. 2) regions. That is, the laminar boundary layer on the cone from the tip to the transition location was generally exposed to noise radiated along Mach lines from transitional or turbulent boundary layers on the nozzle walls at locations far upstream of the test section. Kendall (ref. 9) has noted a similar situation

in the Jet Propulsion Laboratory (JPL) 20-Inch Supersonic Wind Tunnel at a Mach number of 4.5 where transition did not occur on a test plate at a length Reynolds number of 3.3×10^6 when the nozzle-wall boundary layer was laminar. According to reference 10, the nozzle-wall boundary layer in the JPL tunnel can be maintained laminar up to a free-stream unit Reynolds number of 1.8×10^6/m at this Mach number. In order to study transition mechanisms and behavior that occur in the low disturbance environment of flight (ref. 11), a "quiet" wind tunnel with low noise levels at higher unit Reynolds numbers is required (ref. 12).

Various techniques to increase the unit Reynolds numbers at which nozzles can be operated with laminar wall boundary layers are under investigation at the Langley Research Center, including the use of rapid-expansion wall contours, highly polished walls, and boundary-layer bleed slots (refs. 7, 13, and 14). The wall contour shape can influence the development and growth of Görtler vortices which may form over the concave portion of the nozzle walls. There has been considerable speculation concerning the possible involvement of these vortices in the transition process in supersonic nozzle-wall boundary layers (refs. 12, 13, and 15). A recent oil flow study in the slotted, rapid-expansion, Mach 5 nozzle showed that Görtler vortices were present over a surprisingly wide range of Reynolds numbers. This result as well as recently completed calculations of neutral and growth curves for Görtler vortices in supersonic flow by El-Hady and Verma[1] prompted the present reexamination of the possible role of Görtler vortices in transition of the nozzle-wall boundary layers of two Mach 5 nozzles. One of these nozzles is usually referred to as the conventional nozzle and the other as the slotted, rapid-expansion, and/or electroformed nozzle. Detailed data on the mean properties of the free-stream and boundary-layer flow in the former nozzle are available in reference 16. Both the mean and fluctuating properties of the free-stream flow in both nozzles are given in references 7, 13, 14, 17, and 18. Also, some boundary-layer mean-pitot-pressure surveys at the exit of the slotted nozzle are given in reference 14. Obviously, the flow in these two nozzles has been more thoroughly probed and analyzed than in most wind-tunnel nozzles. To establish the free-stream disturbance levels for laminar, transitional, and turbulent wall boundary layers in these nozzles, this extensive data bank will be used. Also some additional data obtained in these nozzles by J. B. Anders of the Langley Research Center but not previously published will be utilized.

This report is limited to a look at the presence and growth of Görtler vortices in both nozzles. Also, the question of how the vortices may be involved in transition of the nozzle-wall boundary layers will be addressed.

SYMBOLS

A disturbance amplitude

c speed of sound, $\sqrt{\gamma RT}$

[1]Work being done by N. M. El-Hady and A. K. Verma, Old Dominion University, Norfolk, Virginia, under contract to Langley Research Center.

f	frequency
G	Görtler parameter, $R_\theta\sqrt{\theta/r_c}$
K	empirical factor (see eq. (A5))
L	nozzle length from throat to exit
ℓ	test rhombus length or wetted flow length on cone (see fig. 18)
M	Mach number
N	average number of waves around nozzle periphery
N_{ref}	number of waves counted between known reference points
n	integrated growth factor
p	static pressure
p_t	pitot pressure
$\mathcal{R}$	ideal gas constant
R	unit Reynolds number
R_ℓ	local Reynolds number based on length ℓ
R_θ	local momentum thickness Reynolds number based on conditions at edge of boundary layer
r	radius
r_c	longitudinal radius of curvature
rms	root mean square
S	ray-tube area for geometric acoustics
s	slot width (see fig. 2)
T	temperature
TS	Tollmien-Schlichting
u	streamwise velocity
x	axial distance from throat
x_o	axial distance from throat to acoustic wave inlet section
x_R	location of upstream tip of test rhombus

α wave number, $2\pi/\lambda$

β amplification rate factor in Smith's spatial theory (see ref. 19)

γ ratio of specific heats

Δx distance of slot lip from "design" location (see fig. 2)

θ momentum thickness

θ_w nozzle wall angle

λ wavelength

ρ density

ω_* dimensionless frequency, $\frac{2\pi f x_o}{c}$

Subscripts:

a acoustic origin

aw adiabatic wall temperature

e local conditions at edge of boundary layer

I inflection point on nozzle wall

o conditions in settling chamber

s slot

T transition

w at surface

∞ free stream in nozzle test rhombus

* nozzle throat

Superscripts:

~ root mean square

- mean value

COMMENTS ON LINEAR STABILITY THEORY AND TRANSITION

Since we are considering the possible effects of boundary-layer instabilities on transition in the nozzles where stream disturbances and wall roughness may be important, a brief review of three types of instabilities and their known sensitivity to disturbances is presented. These three instabilities are Tollmien-Schlichting waves, cross-flow instability leading to streamwise vortices, and centrifugal instability leading to Görtler vortices in concave wall flows.

Tollmien-Schlichting Waves

Linear stability theory for the amplification of Tollmien-Schlichting (TS) waves has now been applied to the correlation and prediction of boundary-layer transition with considerable success for a variety of two-dimensional flows from subsonic to supersonic speeds (refs. 20 to 22). When the levels of the disturbance environment are known and accounted for, even the simple e^n method can provide fairly reliable estimates of transition Reynolds numbers since n usually increases as the disturbance levels decrease (ref. 22). An example of the effect of very low disturbance levels on n is found in the data on an unswept sailplane wing of high quality surface finish in free flight at low Reynolds numbers where the amplification ratio corresponding to transition was about e^{15} (ref. 23).

Mack (ref. 10) has pointed out that if the well-known e^9 criterion of Smith and Gamberoni (ref. 24) is applied to supersonic boundary layers at Mach 2 and 4.5, the corresponding flat-plate Reynolds numbers at transition onset would be 20×10^6 and 10×10^6, respectively. However, this transition Reynolds number for Mach 2 is considerably larger than values measured in flight (ref. 11) on a 10° included angle cone where the end of transition occurred when $R_{\ell,T} \approx 10 \times 10^6$. The corresponding measured stream disturbances were at the extremely low level of $\tilde{p}_{t,e}/\bar{p}_{t,e} = 0.02$ percent. Two of the many possible complicating factors here are the differences between (a) the onset and end of transition and (b) cone and flat-plate transition (ref. 3). An enlightening discussion of these and many other complicating factors and the related uncertainties of transition "prediction" are available in Morkovin's timeless review of 12 years ago (ref. 25).

In the typical environment of supersonic wind tunnels, the turbulent wall boundary layers radiate high level acoustic noise onto the test model. Kendall (ref. 9) has shown that in the JPL 20-Inch Tunnel over the Mach number range from about 3 to 6, the flat-plate laminar boundary layer amplified these free-stream acoustic disturbances in accordance with Mack's forcing theory (ref. 10). At the onset of transition, the resulting measured ratios of disturbance amplitude in the boundary layer to that in the free stream A/A_∞ ranged from about 13 ($n_\infty = 2.6$) to 85 ($n_\infty = 4.4$) depending on the Mach number and the disturbance frequency where

$$n_\infty = \ln A/A_\infty$$

Even though these "overall" amplification ratios include the acoustic "pre-amplification" (Mack's forcing theory, ref. 10) upstream of the neutral stability point, they are still much smaller than values of n in low turbulence, low-speed wind tunnels where transition occurs for amplitude ratios of about 900 ($n = 6.8$) to 180 000 ($n = 12.1$). (See ref. 20.)

On the other hand, when the tunnel-wall boundary layers in the JPL tunnel are laminar, which occurs up to a free-stream unit Reynolds number of $1.8 \times 10^6/m$ for $M_\infty = 4.5$, Mack (ref. 10) noted that the equivalent flat-plate Reynolds number of the laminar wall boundary layer is 27×10^6 although the velocity profile bears no resemblence to the flat-plate profile. Further research on the mechanisms involved in the breakdown of TS waves into transitional flow at supersonic speeds must await the development of a facility where stream disturbances can be controlled and reduced.

Cross-Flow Instability and Streamwise Vortices

Streamwise vortices due to inviscid cross-flow instability in the boundary layer of swept wings were first observed by Gray as discussed in reference 26. The linear equations that govern this three-dimensional instability and its growth rates were derived by Gregory, Stuart, and Walker (ref. 26). Owen and Randall (ref. 27) introduced a cross-flow Reynolds number to correlate the onset of the vortices and the subsequent transition on swept wings in low-speed flow. The cross-flow Reynolds number criteria has also been applied with some success to supersonic flows (refs. 28 and 29). These early results tended to confirm the expectation that the cross-flow instability might not be as sensitive to free-stream disturbances as TS instability since the cross-flow instability could amplify at much higher rates (ref. 26) in typical flows.

Since these early results, the theoretical treatment and computational methods for the cross-flow instability problem have been very considerably advanced (refs. 30 to 32, for example). A recent study of the e^n method applied to cross-flow instability on swept wings (ref. 33) has shown that values of n at transition (without suction) are in the same range (from 6.8 to 11.5) as in the two-dimensional TS cases of reference 20. This result was hardly to be expected since the basic instability mechanisms are entirely different with supposedly different sensitivities or "receptivities" to disturbances. However, due to insufficient data, little can as yet be said about the effect of external disturbances on the values of n for cross-flow instabilities although smaller values of n were computed (ref. 33) for two swept-wing cases with suction. This latter result may imply that suction slots introduce internal disturbances that cause transition at lower amplification ratios. Again, further research into the relation between cross-flow instabilities and transition at supersonic speeds must be conducted in a facility where stream disturbances can be varied over a significant range of levels and spectra.

Görtler Vortices

The centrifugal instability and resulting counterrotating streamwise vortices that form in a laminar boundary layer along a concave surface have

been studied extensively since Görtler (ref. 34) first calculated their neutral stability and growth characteristics. Traces of the Görtler vortices were first observed as uniformly spaced streaks in china-clay lacquer applied to the concave surface of the flap on a Griffith airfoil by Gregory and Walker (ref. 35). Several years before that, Liepmann (ref. 36) had observed that transition occurred on slightly concave walls when $G \approx 7$. These transitional values of G depended also on the levels of turbulence in the free stream (ref. 37).

Smith (ref. 19) rederived the disturbance equations for this stability problem and included terms for the normal velocity and streamwise variations of curvature. He introduced a spatial amplification factor $\beta(x)$ and calculated the amplification ratio to transition for a number of two-dimensional airfoils and test plates from the relation

$$\frac{A_T}{A_{\beta=0}} = e^{n_T}$$

where $n_T = \int_{x_{\beta=0}}^{x_T} \beta(x)\, dx$ and x is the streamwise distance along the surface. He found that n_T varied from about 6 to 12 while the Görtler parameter G was inadequate as an indication of transition since it varied from about 3 to 20 for the same cases. Thus, there is no doubt that the vortices are involved in the transition process. Tani and Aihara (ref. 38) concluded that when the curvature is small, the Görtler vortices affect transition indirectly by inducing spanwise variations in the boundary-layer thickness which promote rapid breakdown of TS waves. This important problem of the interaction of Görtler vortices with TS waves has been studied by Nayfeh (ref. 39) using his method of multiple scales (ref. 40). His results indicate that when both instabilities are present, the vortices provide a very powerful instability mechanism and may dominate the TS effects when the wavelength of the vortices is one-half that of the TS waves.

Comprehensive reviews of the various theoretical approaches to the instability and growth of Görtler vortices are given by Floryan and Saric (refs. 41 and 42). They have shown that extreme care must be taken with the normal velocity terms and computational procedures to obtain reliable results, especially at low wave numbers and small amplification. Ragab and Nayfeh (ref. 43) have shown that when the curvature changes rapidly in a region of favorable pressure gradients, the use of Blasius profiles or even local similarity Falkner-Skan profiles overpredict the growth rates of the vortices by great amounts. While their results are normalized with the Blasius length scale which depends only on the wetted flow length and unit Reynolds number, conversion to the preferred momentum thickness length scale (refs. 19 and 34 to 37) would not have much effect since the Blasius profiles even show wrong trends, predicting increasing growth rates in the favorable pressure gradient region while the correct nonsimilar profiles predict growth rates of the vortices going rapidly to zero. Indeed, these highly nonsimilar local

effects of rapidly changing curvature and favorable pressure gradients may be more important for supersonic nozzle flows than the effects of compressibility. The growth and wave number of the vortices will also depend on whether the nozzle is axisymmetric or two-dimensional.

The neutral stability curves for supersonic flow have been computed by Kobayashi and Kohama (ref. 44) using flat-plate profiles and the Sutherland viscosity-temperature relation. The effect of Mach number on the neutral stability curves was quite significant, especially at the low wave numbers and showed that the stability increased as the Mach number was increased. They stated that for the insulated wall case, this stabilizing effect was due to the increase in viscosity in the wall regions due to the higher temperatures there as compared with those in the free stream, yet there was very little effect of changes in T_w/T_∞ from 0.5 to 5 at Mach 5. As will be seen in the following discussion of the present results, the actual growth paths, or history, of the vortices may be the dominant factor in the wall boundary layers of axisymmetric supersonic nozzles.

APPARATUS AND TESTS

Facility

A description of the blow-down facility used to test the two nozzles, including a dimensional sketch of the high-pressure piping system, is given in reference 13. The supply air is compressed to a maximum pressure of about 35 MPa (5000 psi) and then dried by passing through beds of aluminum oxide desiccant where the dew point is reduced to about 227 K (-52°F). The air is then passed through filters rated to withhold 98 percent of particles 5 μm or larger in size before storage in the high-pressure tank field. A run is started by first opening the vacuum valves to a 3200-m^3 (113 000-ft^3) vacuum sphere. High-pressure air from the tank field is then reduced to a pressure of about 4 MPa (600 psi) by a single stage reducing valve and it is then heated electrically to a maximum temperature of 760 K (500°F). The air enters the blow-down facility through a 25.4-cm (10-in.) diameter supply header. Branching from this header is a 10.2-cm (4-in.) diameter pipe leading to parallel 10.2-cm (4-in.) and 2.54-cm (1-in.) flow control valves as illustrated in figure 4 of reference 13. For most of the present tests, the stagnation temperature was maintained at about 366 K (200°F) and the stagnation pressure was varied from 207 kPa (30 psia) to 1400 kPa (200 psia).

The aluminum oxide dryers were mentioned because of the small residual amounts of powder that pass through the main filters and the settling chamber filter paper (ref. 13) to form random patterns and thicknesses of deposits on the nozzle throat regions. These deposits had a significant effect on transition in the conventional nozzle as described in reference 17 and may also have had some effects on transition in the slotted nozzle (ref. 14). The high-pressure piping system and the facility control valves cause very high acoustic noise levels at the entrance to the settling chambers except at high pressures when the large valve is wide open with subsonic flow through its ports (refs. 13 and 45).

The small settling chamber used during early tests with the conventional nozzle (refs. 45 and 46) was only 14 cm (5.5 in.) in diameter and 30.5 cm (12 in.) in length and was equipped with an entrance diffuser cone, porous plates, a honeycomb, and screens that could be used in various combinations or deleted entirely. Disturbance levels and spectra were measured in the small settling chamber with hot-wires (ref. 45) and pitot-pressure transducers (refs. 17 and 45). The results showed high vorticity levels, as computed from hot-wire mode plots, of 1 to 7 percent. The rms pressure fluctuation levels were also high and varied from about 0.06 to 0.5 percent of the stagnation pressure, depending on the screen configuration. The highest levels were measured when all settling chamber components were removed. Even the lowest levels were considerably larger than those measured in the "big" settling chamber (ref. 13) used with the slotted nozzle. Spectra shown for the small settling chamber in reference 46 indicated high level spikes at high frequencies that probably were acoustic disturbances caused by choked flow conditions in the control valves. The relatively open mesh of the porous plates and the small size of the chamber itself are now believed to be the main reasons for the high disturbance levels in the small settling chamber. That is, the known high input levels of acoustic disturbances were not effectively attenuated by the small Δp porous plates while the short chamber length and the three 50-mesh screens did not provide any significant reduction of the inherently high vorticity levels. The behavior of transition in the wall boundary layer of the conventional nozzle was affected by the screen configuration in these early tests (ref. 45). Of equal importance for the quiet tunnel program was the finding reported in reference 46 that transition on a 5° sharp cone was affected rather strongly by the screen configuration. These results served to emphasize the importance of good settling chamber design on the optimum performance of supersonic quiet tunnels and led to the improvements utilized in the big settling chamber.

The big settling chamber is 2.5 m (100 in.) long and 29.2 cm (11.5 in.) in diameter. Detailed dimensions and specifications of all components in this chamber are given in references 13 and 47. This chamber was used for all tests of the slotted nozzle and by means of a 10.08-cm (4.00-in.) thick adapter flange which provided a smooth contraction from the large chamber to the 14-cm (5.5-in.) inside diameter of the small chamber (fig. 1 of ref. 13), the big chamber was also used for all recent tests of the conventional nozzle that will be reported herein. For these tests, all components were removed from the small chamber.

The big chamber contains a porous entrance cone, a perforated plate, a section filled with steel wool, filter paper, a porous plate, and seven screens. The steel wool and porous components reduced the input noise measured by pressure transducers flush with the wall from 0.3 percent (ref. 13) to 0.004 percent measured with the same type of pressure transducer mounted flush with the wall just upstream of the nozzle entrance (ref. 47). The streamwise velocity fluctuations measured with a hot wire were between 0.2 and 0.4 percent (refs. 13 and 47). If the hot-wire velocity fluctuations are assumed to be plane acoustic waves moving along the length of the chamber, the resulting calculated pressure fluctuation levels are nearly the same as the levels measured at the wall with the pressure transducer (ref. 47). This result is interpreted as an indication that the vorticity levels in this chamber are small (ref. 48).

The velocity fluctuation levels in this chamber were increased to a peak of about 0.9 percent by removing the steel wool. Most of this increase consisted of high-frequency acoustic disturbances (refs. 7 and 13); however, there was no measurable effect of this increased settling chamber noise on transition in the wall boundary layer of the slotted nozzle or on the Mach 5 free-stream noise levels over the entire range of operating pressures (ref. 13).

Nozzles

Sketches of the two nozzles tested, with nominal dimensions and the maximum wall angles included, are given in figure 1. An accurate listing of these dimensions and other pertinent data on the nozzles are given in table I. A complete set of measured wall coordinates and the corresponding inviscid wall Mach number values for the conventional nozzle are tabulated in reference 16. The final smoothed design coordinates for the electroformed nozzle and the corresponding values of M_e are given in table II. Differences between the smoothed design coordinates and the actual measured coordinates are given in reference 13.

Figure 2 shows a scaled drawing of the throat region in the slotted nozzle. The purpose of the boundary-layer bleed slot is to remove the turbulent boundary layer that develops on the settling chamber walls and thereby help maintain a laminar boundary layer at higher Reynolds numbers in the supersonic part of the nozzle (ref. 13). The leading edge of the slot on the electroformed nozzle, which was used for all the present tests, is blunted with a leading-edge radius of 0.25 mm (0.01 in.). The transonic inviscid throat contour downstream of the slot was designed by the method of Hopkins and Hill (ref. 49). The ratio of the longitudinal radius of curvature at the throat to the radius of the throat was taken as unity. Some of the constant Mach number contours computed by this method are shown in figure 2. The supersonic part of the nozzle contour was computed by the method of characteristics with input flow conditions supplied just downstream of the sonic line from the Hopkins-Hill transonic solution and a faired Mach number distribution along the center line with continuous first and second derivatives. The subsonic approach section was designed by an inviscid stream tube calculation which extended the Hopkins-Hill wall streamline to the outer boundary of the slot. The design flow in the slot channel at its minimum width s was sonic to minimize the propagation of any plenum disturbances into the nozzle flow. This design condition requires that the ratio of the slot plenum pressure to the stagnation pressure must be at or below the sonic value of 0.528. The value of s was determined by the requirement that the slot would remove all the mass flow in the upstream boundary layer plus enough of the nominal inviscid flow to allow intermittent turbulent bursts in the outer part of the boundary layer to flow into the slot. In any case, the value of s can be adjusted by axial movement of the nozzle with respect to the approach section as indicated by the approximate formula for s given in figure 2. For all the present tests, $\Delta x = -0.036 r_*$ which is the optimum value for transition in the nozzle-wall boundary layer (ref. 13). Details on the boundary-layer calculations used in the nozzle design are given in reference 15. The inviscid contour downstream of the slot lip was "corrected" to allow for boundary-layer flow by adding the values of displacement thickness to the radius. The displacement thickness was calculated for a laminar boundary layer

by the method of reference 50 for a stagnation pressure of 1034 kPa (150 psia) and a stagnation temperature of 378 K (680°R).

Oil Flow Technique

For the oil flow studies on the conventional nozzle and during the early part of the present program, titanium oxide powder was mixed into silicone oil of 0.0001 m^2/sec (200 cs) viscosity until a smooth mixture with the consistency of light cream was obtained. This mixture was applied uniformly over the portion of the nozzle surface to be photographed. The photographs of the nozzle exits were made with the camera axis at an angle of about 30° to the nozzle center line so that the downstream part of the nozzle surface on one side was visible. Due to problems with insoluble clumps of the titanium oxide powder, a fine organic powder (ref. 51) used as a pigment in flourescent paint was used later in the program. A mixture by volume of 1 part powder to 2 parts silicone oil was used for all the present photographs of the slotted nozzle.

After application of the oil mixture the desired stagnation pressure and temperature were established within about 5 sec after the start of a run and then were held steady for 1 to 3 min, depending on the viscosity of the mixture and the run conditions. After the pattern was observed to stabilize, the facility control valves were closed to end the run. Close observation of the oil flow pattern during the run shutdown period showed that the pattern remained fixed due to partial drying and hardening of the mixture. In fact, with the proper mixture and exposure time the pattern would remain fixed for 2 to 3 days after tunnel shutdown.

FREE-STREAM DISTURBANCE LEVELS

The free-stream disturbance levels measured along the center line of the nozzles and the time variation of the corresponding hot-wire or pressure-transducer signals (refs. 7, 13, 14, 17, 18, and 45) have been used to determine if the boundary-layer flow on the nozzle walls is laminar, transitional, or turbulent. The flow sources of these measured disturbances are located in the vicinity of the "acoustic origin" which is the locus of intersection of a Mach cone (with its tip at the probe) and the wall or near-wall region of the boundary layer that radiates the noise. Thus, for a probe on the center line, the acoustic origin locations would be along a meridional curve around the periphery of the nozzle as illustrated in the upper part of figure 1. At low Reynolds numbers where the boundary layer at the acoustic origins is laminar, the acoustic disturbances sensed by the probe consist of noise propagated directly from the settling chamber and noise caused by "shimmering" Mach waves which are detected as stationary sources by a hot wire. The shimmering waves come from oscillations of the laminar boundary layer generated by the convection of instability waves or any unsteadiness over wall roughness and waviness. When the boundary layer at the acoustic origins is turbulent with local free-stream Mach numbers above about 2.5, then the measured noise levels increase by 1 or 2 orders of magnitude due to the interaction of turbulent eddies moving at supersonic speeds relative to the free stream. This type of acoustic disturbance was first elucidated by Laufer (ref. 52) and is caused by

eddy waveletts which are propagated along Mach lines. Both the laminar and turbulent noise emission mechanisms as manifested in the conventional and slotted nozzles were discussed in detail in reference 13.

Typical estimated values of local vorticity disturbances and noise transmitted from the settling chamber are presented in the appendix, where it is shown that these disturbance modes are less than 0.01 percent due to low disturbance levels measured in the big settling chamber. Plausible speculations regarding noise contributions from shimmering Mach waves are also offered in the appendix. Again, this type of noise that is incident upon the laminar boundary layer at the acoustic origins is likely to be the order of 0.01 percent at low unit Reynolds numbers. At higher unit Reynolds numbers, the noise levels probably increase due to the thinner boundary layers and to increased amplitude of instability waves. Thus, the levels of the following center-line disturbances are not directly related to local incident disturbances but they are presented here to emphasize the differences in these levels for laminar and turbulent boundary layers and to provide the basic data used to determine the precise locations and unit Reynolds numbers for transition in the nozzle-wall boundary layers.

Conventional Nozzle

Figure 3 shows the variation with R_∞ of rms static-pressure fluctuations normalized with the mean static pressure as obtained from hot-wire measurements at several points along the center line of the conventional nozzle. The data in figure 3(a) (from ref. 13) are from a unique set of measurements made when the throat region of this nozzle was freshly polished and cleaned at frequent intervals. When the throat was maintained in this condition, transition moved upstream as R_∞ was increased; that is, at a given value of R_∞, such as 10^7/m, transition was detected first at the farthest downstream station corresponding to $x_a/L = 0.737$. At the higher value of $R_\infty \approx 1.5 \times 10^7$/m, transition was finally detected at the upstream station corresponding to $x_a/L = 0.363$. The test procedure was to place the probe at a given station and increase the value of R_∞ in small increments by increasing the stagnation pressure in small steps. The first pressure at which abrupt spikes were detected in the hot-wire signal then corresponds to the transition value of R_∞ at that probe station since the spikes were caused by noise radiated from turbulent bursts in the nozzle-wall boundary layer at the corresponding acoustic origin (ref. 47). Note that as R_∞ is increased further, the rms values increase very rapidly indicating the passage of increasing numbers of turbulent bursts through the acoustic origin locus. The normalized rms values then reach a peak and subsequently decrease corresponding to the development of fully turbulent flow.

Figure 3(b) shows an entirely different type of transition behavior that was usually observed (refs. 16, 17, and 45) in this nozzle when no special effort was made to polish or clean the throat.[2] That is, at $R \approx 8 \times 10^6$/m,

[2]The data in figure 3(b) for R_∞ 10^7/m were previously published in reference 18; the data for $R_\infty < 10^7$/m were from the same test series but have not been published before.

transition was observed at all stations in the nozzle which indicates that transition suddenly "jumped" upstream to at least $x_a/L = 0.190$ at this value of R_∞. This sudden upstream movement of transition can probably be attributed to roughness in the throat region where the boundary-layer thickness is about 0.2 mm (0.01 in.) thick (ref. 16) at this value of R_∞.

On the other hand, when the nozzle walls are cleaned and polished, transition moves upstream gradually with increasing R_∞ and transition could then be dominated by Görtler vortices. Since the concern herein is with the possible effects of Görtler vortices on transition, only the transition data from figure 3(a) are used in the following sections of this report.

Slotted Nozzle

Figure 4 shows the normalized rms static-pressure fluctuations in the slotted nozzle with the bleed valves open, obtained and plotted in the same way as for the conventional nozzle. Figure 4(a) utilizes the data given in references 7 and 13 as the ratios of rms pitot pressure to mean pitot pressure but shown here in terms of the corresponding static pressures. The equation used to relate the pitot and static-pressure fluctuations is given in reference 47. The movement of transition from $x_a/L = 0.839$ to 0.152 is similar to that in the polished conventional nozzle (fig. 3(a)). That is, transition moved upstream gradually into the nozzle as R_∞ was increased. Although the location of transition in this nozzle was affected by throat roughness and deposits (ref. 14), the gradual upstream movement of transition with increasing R_∞ was always observed in this nozzle, at least up to $x_a/L = 0.152$. This behavior of transition probably indicates that wall roughness did not dominate transition for $x_a/L > 0.152$.

Additional new data at stations further upstream in the slotted nozzle are shown in figure 4(b). These data indicate that transition occurred at the far upstream stations of $x_a/L = 0.073$ to 0.027 without any consistent spatial movement and usually at the nominal unit Reynolds numbers of $R_\infty \approx 2 \times 10^7/m$ or $2.6 \times 10^7/m$. The boundary layer at these upstream stations for these high Reynolds numbers is extremely thin and therefore highly sensitive to slight variations in local roughness and dust deposits.

Spatial Variation of Noise Levels

The variation of the normalized rms static-pressure fluctuations along the center line of both nozzles is shown in figure 5 for two values of R_∞. The flagged symbols are for data in the conventional nozzle for both the polished and rough throat and the unflagged symbols represent data in the slotted nozzle.

At the lower value of R_∞, $5 \times 10^6/m$, the wall boundary layer at all the listed acoustic origins (figs. 3 and 4) was laminar in both nozzles. The corresponding noise levels (fig. 5) range from about 0.015 percent to 0.25 percent with the lower values observed in the polished conventional nozzle at $x \approx 37$ cm and over the middle section of the slotted nozzle from about $x = 25$ to 35 cm. The higher laminar levels above 0.07 percent in the unpolished conventional

nozzle may be caused by wall roughness in the form of aluminum oxide deposits. In the slotted nozzle, the higher laminar levels for $x < 20$ cm are caused by the previously noted (ref. 18) axisymmetric machining errors and roughness effects in the throat region where the laminar boundary layer is only about 0.1 mm (0.005 in.) thick for this value of $R_\infty \approx 5 \times 10^6/m$. The higher laminar levels for $x > 40$ cm in the slotted nozzle may be caused by increasing amplitude of unstable oscillations in the laminar boundary layer preceding transition in the downstream regions of the wall boundary layer. (See ref. 13 and the appendix.)

Figure 5 shows that at the higher value of R_∞, $50 \times 10^6/m$, the boundary layers were always turbulent and the normalized rms values range from about 0.15 percent to nearly 3 percent depending primarily on the location in the nozzle and the corresponding values of M_e at the acoustic origins (ref. 18). The data in the slotted nozzle with bleed valves closed may be compared with the levels for bleed valves open. This comparison shows that for x from about 15 to 25 cm, the rms levels are higher with the bleed valves open than closed probably because of transitional burst effects still present in the upstream regions even at this high Reynolds number. As noted previously, the purpose of the boundary-layer bleed slot was not to reduce the noise at high Reynolds numbers where the boundary layer is already turbulent but to help maintain laminar boundary layers in the supersonic part of the nozzle at higher Reynolds numbers than otherwise possible. The important point to be made from this figure as discussed in the appendix, is that the local disturbance levels incident on the laminar boundary layer for $R_\infty \approx 5 \times 10^6/m$ at the upstream acoustic origins are probably below the minimum measured center-line values of 0.015 percent which is in the range of disturbance levels measured in flight (ref. 11).

RESULTS AND DISCUSSION

Basic Transition Data

The method of detecting transition as described previously is probably one of the most sensitive techniques for supersonic boundary layers since even a single turbulent eddy that passes through the acoustic origin locus anywhere on the nozzle periphery can be easily detected on the oscilloscope. It follows that any localized roughness area or irregular deposits of dust on the nozzle surface could induce turbulent bursts downstream of that area even when TS waves or Görtler vortices may be dominant factors elsewhere. The data for the first pressure at which the signal bursts were observed thus represent the earliest onset of transition for the particular conditions of the test. These conditions include not only the degree of wall polish and cleanliness but also the wall temperature. Data given in references 13 and 17 show that transition in both nozzles was indeed sensitive to the wall temperature. For the data used in this report, $T_w \approx T_{aw}$. Although precise wall temperature measurements are not available, the approximate range for the present tests is $0.95 < \frac{T_w}{T_{aw}} < 1.0$.

With these limitations in mind, the transition data from figure 3(a) for the conventional nozzle and figures 4(a) and 4(b) for the slotted nozzle are shown in figure 6. The free-stream unit Reynolds number at which the turbulent bursts were first observed is plotted against the probe location on the nozzle center line and also the corresponding acoustic origin location which is, of course, the local transition "point." It is evident that the data follow reasonably consistent trends which are similar for both nozzles except the data for $x < 3$ cm in the slotted nozzle. These latter data points are too close to the throat to have been affected by any significant length of concave curvature and are subject to very slight changes in any of these conditions of roughness or wall temperature. Before further discussion of transition Reynolds numbers and some detailed consideration of local conditions for the formation and amplification of Görtler vortices are presented, typical oil flow results are examined.

Oil Flow Photographs

Conventional nozzle.- Some of the oil flow photographs from reference 12 taken at the entrance and exit of the conventional nozzle are shown in figure 7. These photographs were taken before the nozzle throat was polished; nevertheless, at the low Reynolds number of 5.6×10^6/m the regularly spaced streaks at the exit show clearly that Görtler vortices were present. The data of figure 3(b) show that the boundary layer up to at least $x_a/L \approx 0.53$ would be laminar at this Reynolds number. In fact, because of the simultaneous occurrence of transition at all probe stations for $R \approx 8 \times 10^6$/m it can be assumed that the entire length of the nozzle boundary layer was laminar at $R_\infty = 5.6 \times 10^6$/m. The photograph at this lower Reynolds number of the nozzle entrance shows that vortices were also present there and appear to persist for some distance into the convex portion of the approach which, from figure 1, would occupy most of the central region of the nozzle entrance photograph.

At the higher Reynolds number of 1.2×10^7/m, clearly discrete streaks can no longer be seen. Since the wall boundary layer is completely turbulent at this Reynolds number (fig. 3(b)), the laminar Görtler vortices have presumably been obliterated by the relatively long run of turbulent flow in the conventional nozzle.

Slotted nozzle.- Oil flow photographs at the exit of the slotted nozzle with bleed valves open and closed at four Reynolds numbers are shown in figure 8. With bleed valves open the streaks are present up to $R_\infty \approx 1.4 \times 10^7$/m and the average spacing (or wavelength) of the streaks appears to increase with increasing Reynolds number. At the highest Reynolds number of 2.7×10^7/m, the widely spaced discrete streaks are not seen. In the original photograph very fine closely spaced streaks with a random pattern could be seen. Repeat runs made over a period of about 2 months, and also after a lengthy polishing effort was made, showed that these fine streaks were caused primarily by pits and scratches in the surface over the downstream 10 to 15 cm of the nozzle. Small clumps of powder in the oil mixture would also occasionally cause fine random streaks.

When the bleed valves were closed, the widely spaced streaks disappeared over the entire range of R_∞. Again, the fine closely spaced streaks are observed that are similar to those at $R_\infty \approx 2.7 \times 10^7/m$ with bleed valves open. It is thought that some of these fine streaks may be evidence of Görtler vortices in turbulent flow (ref. 53); however, no consistent count of streaks per unit width of the nozzle-wall surface could be obtained probably because of the interference due to background roughness and powder clumps which can be clearly seen, for example, in figure 8(b) for bleed valves closed. Tests before and after polishing the nozzle surface indicated the roughness in this downstream region had no effect on the streak patterns observed with bleed valves open.

However, the streak pattern with bleed valves open at intermediate values of R_∞ did occasionally change for different runs at the same test conditions over periods of several days. An example of this type of streak pattern change is shown in figure 9 for $R_\infty \approx 1.4 \times 10^7/m$. Comparison of the two photographs at the top of the figure shows the streak pattern in the upper part of the oil film region in the vicinity of the upper pressure orifice (indicated by the arrow in photograph on left) is essentially the same. However, the pattern in the vicinity of the lower pressure orifices in the lower half of the photograph is completely different in these two photographs. These changes may be attributed to small changes in dust deposits in the upstream regions of the nozzle or even near or on the nozzle lip itself. The photograph at the bottom of figure 9 shows evidence of completely turbulent flow over the upper portion of the oil film region where the widely spaced streaks are not seen, whereas the remaining streak pattern in the lower region is different from that in the other two photographs. This latter change in the streak pattern seems to be consistent with changes in the transition Reynolds number as reported in reference 14 and was apparently caused by variations in dirt deposits in the throat region.

One final point to be made about the streak patterns in the slotted nozzle with bleed valves open is the apparent persistence of the streaks into the downstream regions of the nozzle even when the onset of transition has occurred far upstream. Thus, for example, at $R_\infty \approx 1.4 \times 10^7/m$, the "tracks" of the Görtler vortices are clearly evident at the nozzle exit in figure 8(c) with bleed valves open, but according to data shown in figures 4 and 6 the onset of transition has already occurred about 30 cm upstream at this value of R_∞. Furthermore, the trend of the normalized rms data with R_∞ in figure 4(a) would indicate that from $x_a/L \approx 0.8$ to 1.0, the nozzle boundary-layer flow should be completely turbulent. It can only be concluded that either the vortices, once they are formed and growing, do indeed persist far into the downstream turbulent flow or that the wall boundary layer there is still in some transitional or quasi-turbulent state.

Wave Number of Oil Flow Streaks

In an attempt to relate the oil flow streaks to Görtler vortices, it is useful to determine the apparent average wave number of the streaks. This has been done for a number of runs with the slotted nozzle by simply counting the number of streaks between reference points that are a known distance apart around the periphery of the nozzle and assuming that the resulting average distance between the streaks is the wavelength of the vortices. Except for

slight errors due to occasional misalignment of the streaks with the fixed reference points, this assumption implies that the oil flow process causes the oil to accumulate in a streamwise streak between each pair of counter rotating vortices where the converging streamlines from adjacent vortices carry the flow away from the surface. (See diagram of streamline patterns in ref. 19.) The upper and lower pressure orifices visible in figures 8 and 9 (indicated by arrows in fig. 8(a), bleed valves open, and in fig. 9 in the upper left-hand photograph) are 5.41 cm apart; therefore, the average wavelength in centimeters was then taken as

$$\lambda = \frac{5.41}{N_{ref}}$$

where N_{ref} is the number of waves (streaks) between the orifices. The results from several runs where the streaks were uniformly visible are plotted in figure 10 as the wave number $\alpha = 2\pi/\lambda$ against R_∞. The trend of decreasing wave number with increasing R_∞ is clearly apparent in spite of the fairly large scatter. For values of $R_\infty > 2.2 \times 10^6$, the widely spaced streaks were never seen and as mentioned previously the large increase in wave number corresponding to the fine, closely spaced streaks (two typical values at $\alpha \approx 27$ and 33 are included in the figure) may be attributed partly to local roughness of the nozzle surface. The flagged points in the figure are used later in the report for another purpose but it is worth mentioning here that the two flagged points at $R_\infty = 0.46 \times 10^7$ and 0.88×10^7 happen to be taken from figures 8(a) and 8(b), respectively.

The only oil flow photographs available for the conventional nozzle are those published in reference 12, four of which are given in figure 7. The wave number for $R_\infty = 5.6 \times 10^6/m$ at the exit of the nozzle from this figure is $\alpha \approx 43.5\ cm^{-1}$ which is about twice the values in the slotted nozzle. As shown later, this large difference is not related to the differences in boundary-layer thickness parameters in the two nozzles. Before computing amplification ratios for the Görtler vortices, typical variations in momentum thickness and the Görtler parameter, $G = R_\theta \sqrt{\theta/r_c}$, with distance from the throat are presented.

Variations in M_e, θ, G, and R_θ With x

The variation of the local inviscid Mach number M_e along the wall with x, the axial distance from the throat, for the slotted and conventional nozzles is shown in figures 11(a) and 11(b), respectively. Values of momentum thickness θ and G computed for laminar boundary layers by the method of reference 50 at $R_\infty = 1.35 \times 10^7/m$ for the slotted nozzle (fig. 11(a)) and at $R_\infty = 1.2 \times 10^7/m$ for the conventional nozzle (fig. 11(b)) are also shown. Values of R_θ for these Reynolds numbers in the two nozzles are plotted against x in figure 12. The locations of transition at these Reynolds numbers are noted in the figure. The computed laminar values of these boundary-layer parameters would not apply for $x > x_T$.

Since the Görtler vortices cannot form until $G > 0$ and become unstable or begin to grow for larger values of G (around $G = 0.3$ to 1.0 depending on the wavelength and local Mach number in the neutral stability theory for flat-plate profiles (ref. 44)), it can be seen from figure 11 that the vortices downstream of the throat would have large streamwise distances to amplify and disturb the laminar boundary layer upstream of transition for the two examples shown in this figure. In the supersonic region of the nozzles it may also be noted that for $G \approx 1.0$ where the vortices would begin to amplify, the local Mach number in both nozzles is between 2 and 3. In the subsonic portion of the conventional nozzle, figure 11(b) shows that for $R_\infty = 1.2 \times 10^7/m$, G increases very rapidly to a peak value of about 8.5 at $x \approx -10$ cm. These large values of G presumably account for the streamwise streaks (indicating the presence of vortices) in the subsonic approach that are clearly visible in figure 7(a) at the lower Reynolds number of $5.6 \times 10^6/m$. (Since G is proportional to the 1/4 power of Reynolds number, the peak value of G is only reduced to about 7 at this lower Reynolds number.) However, since G rapidly returns to zero at the start of the convex portion of the approach, it is assumed for the present purposes that these vortices are rapidly damped as they pass through the convex nozzle throat and have no direct effect on the new downstream vortices. Of course, it is possible that some residual disturbances from these subsonic vortices may influence the formation or wavelength of the new vortices that would begin to develop at about 9 cm downstream of the throat where G again begins to increase. One of the original purposes of the slotted nozzle (refs. 12 and 15) was to remove all such traces from the downstream supersonic boundary layer by placing the slot lip at or downstream of the inflection point in the subsonic approach as illustrated in figures 1 and 2.

Values of G and R_θ at Transition

The local values of G and R_θ at the acoustic origin locations for transition from figure 6 are plotted against x_a in figure 13. For $x \geq 9$ cm, where the vortices should be fully developed, $R_{\theta,T}$ varies by about 24 percent from 800 to 1050, whereas G_T only varies by about 12 percent from about 5.3 to 6. This range of values of G_T may be compared with the range for low-speed flows of about 3 to 20 (ref. 19). Thus, in the sense of minimum variation of the transition parameter, G_T could be considered to give a "better" correlation of transition data than G in low-speed flows or R_θ for the present data. For values of $x < 9$ cm, G cannot be considered as a consistent correlation parameter for transition in the slotted nozzle since the values of G_T vary from about 2.8 to 5.1. This result is taken to be simply an indication that factors other than the vortices are involved in the transition process for these small values of x.

Amplification of Görtler Vortices

As mentioned previously, Smith (ref. 19) showed that the value of the exponent n in the amplification ratio e^n provides a much better index for transition than G on concave wings and plates. To minimize the effects of the profile shapes on the computed neutral stability and growth curves for Görtler vortices, the curves are usually presented (refs. 34 and 19) as plots

of G against dimensionless wave number $\alpha\theta$, where θ is used as the normalizing length parameter. Some limited results at $M_\infty = 2.2$ of extensive calculations[3] for neutral stability and growth rates of Görtler vortices in supersonic flow are shown in figure 14 in the terms of these parameters. These calculations are for a stagnation temperature of 310 K with adiabatic wall temperature and flat-plate boundary-layer profiles. The maximum amplification curve is the locus of the minimums on the constant growth rate curves. Comparison of the neutral stability curve with that of reference 44 at $M_\infty = 2.0$ and $T_\infty = 273$ K shows reasonable ageement considering the differences in temperature conditions.

The upper set of data points in figure 14 are the computed laminar values of G plotted against $\alpha\theta$ near the slotted nozzle exit corresponding to the values of R_∞ and the observed α for the four flagged points in the wave-number plot of figure 10. The lower set of larger symbols represent the local computed values of G and $\alpha\theta$ near the upstream end of the growth path where α is computed by assuming that N, the total number of waves around the periphery of the nozzles, remains constant at the observed value near the exit based on the counted average there as described previously. The two lines connecting pairs of upper and lower points are simply the computed values of G and $\alpha\theta$ for the laminar boundary along the slotted nozzle wall where N was assumed constant at 95 and 135 as obtained from the corresponding points in figure 10 for $R_\infty = 1.35 \times 10^7$/m and 0.46×10^7/m, respectively, with r = 6.43 cm. (See table II.) When the upper data points are near the maximum amplification curve, the growth path might be expected to result in nearly the maximum amplification rates. However, when these points are farther away from the maximum amplification curve, the growth rates could be considerably smaller than the maximum. The effect of these different growth rates on n will be considered in the following paragraphs.

For the purposes of the present discussion, the procedure used in reference 54, where the amplification of Görtler vortices in supersonic nozzles was computed in detail for the first time, will also be used herein. This procedure is the usual straight-forward approach of disregarding any wave-number restrictions near neutral stability or during the downstream growth of the vortices and to simply assume that maximum amplification occurs along the entire growth path length. It is then convenient to plot the variation of the dimensionless growth rate parameter $\beta\theta R_\theta$ for maximum amplification against the Görtler parameter G as done in reference 54. Typical maximum amplification curves for incompressible flow based on results given in references 19 and 42 are given in figure 15. Included for comparison are corresponding curves based on the unpublished computations of El-Hady and Verma at $M_\infty = 2.2$ and 5. For $G < 1$, the various curves differ considerably but for $G > 1$ where most of the amplification will occur, the curves for incompressible flow tend to converge and the two curves for supersonic flow are somewhat lower and about the same for both Mach numbers up to G = 10. To illustrate the smaller growth rates

[3]Stability calculations made by N. M. El-Hady and A. K. Verma. The method used is similar to that of reference 43 wherein the first-order effects of boundary-layer growth and streamwise variation of mean flow quantities are included.

that would occur with the assumption of a fixed number of waves in the slotted nozzle, Smith's (ref. 19) constant growth rate curves were used along with the growth paths from figure 14 to construct the corresponding amplification rate curves shown in figure 15 for $R_\infty = 0.46 \times 10^6/m$ and $1.35 \times 10^6/m$. It is evident that the amplification for the growth path at $R_\infty = 1.35 \times 10^6/m$ will be considerably smaller than for any of the maximum amplification curves. The amplification for $R_\infty = 0.46 \times 10^6/m$ will be much closer to those for the maximum amplification curves.

Typical values of β normalized with r_*, the nozzle throat radius, are shown plotted against x in figure 16 for the slotted nozzle and conventional nozzle at $R_\infty = 1.35 \times 10^7/m$ and $R_\infty = 1.2 \times 10^7/m$, respectively. For $x > 0$, in the supersonic flow, the maximum amplification rates obtained from the Floryan and Saric (incompressible) and El-Hady and Verma ($M_\infty = 2.2$) curves of figure 15 are given. The integrated growth to the transition location of the vortices is then given by[4]

$$n_T = \int_{x_{\beta=0}}^{x_T} \beta r_* \, d\frac{x}{r_*}$$

It is now apparent from figure 16 that the El-Hady and Verma compressible values of β will give smaller values of n_T for both nozzles than the incompressible Floryan and Saric values as would be expected from figure 15. However, a much larger effect on n_T will obviously result from the use of the actual growth path for $R_\infty = 1.35 \times 10^7/m$ from figure 14 for the slotted nozzle. The growth path in figure 14 for the smaller unit Reynolds number of $0.46 \times 10^7/m$ will not be used since no measured location of transition was available for this Reynolds number (fig. 6). The variation of βr_* for the subsonic part ($x < 0$) of the conventional nozzle is included in figure 16 as a matter of interest, but no transition data are available for this part of the nozzle. The relatively large value $n = 12.5$ obtained by integration of the βr_* curve for $x < 0$ suggests that transition could have been triggered by the subsonic vortices in this part of the nozzle.

The computed values of n_T over the Reynolds number range from the various maximum amplification curves are plotted in figure 17 against x_T corresponding to the observed location of transition at the acoustic origin points. The large increases of n_T with increasing x_T for both nozzles may be caused indirectly by residual wall roughness, dust deposits, and machining errors all of which would tend to remain of some absolute fixed size throughout the nozzle. These wall defects would offer decreasing relative disturbances with increasing

---

[4]The indicated integration should be carried out along the conventional boundary-layer surface coordinate rather than the axial distance x. However, all flow variables and transition locations are given in terms of the axial coordinate x; therefore, for the present purposes, this was taken as the variable of integration. The resulting maximum errors in n occur for small values of x_T in the slotted nozzle where the following computed values of n_T are about 5 percent too small.

x_T not only because the boundary layer gets much thicker with increasing downstream disturbance but also due to the decreasing unit Reynolds numbers with increasing x_T. (See figs. 3(a) and 4(a).) The considerably smaller values of n_T for the conventional nozzle compared with those for the slotted nozzle could conceivably be related to the larger disturbance levels in the conventional nozzle. That is, since the conventional nozzle has no slot to remove the upstream boundary layer originating in the settling chamber, the laminar boundary layer observed in the supersonic part would be subjected to any residual disturbances such as those from the Görtler vortices that would be present in the subsonic approach at the lower Reynolds numbers (figs. 7(a), 11(b), and 16). At the higher Reynolds numbers, the supersonic laminar boundary layer must be the product of a relaminarized turbulent boundary layer and hence might be expected to have rather high external vorticity disturbances left over from the upstream relaminarization process. These possible "explanations" of the trends and differences in n as shown in figure 17 are obviously highly speculative. Thus, the increasing values of n_T with increasing downstream distance may simply imply that amplification of the vortices is not a dominant factor in transition. The fact that G_T is nearly constant for $x \geq 6$ cm from figure 13 may therefore be coincidental. However, it seems more likely that the available linear instability calculations are inadequate for these axisymmetric nozzle boundary layers where the actual growth rates may be modified drastically by the large favorable pressure gradients and to some extent by the geometry of the nozzle surface. Some indication of the effects of the geometry and the actual growth path in terms of the variation of G with $\alpha\theta$ is apparent from the sample case worked out for the slotted nozzle. Thus, when the Smith (ref. 19) amplification curves are used, n_T is reduced from about 15 to 6.7 (fig. 17) by using local values of θ and R_θ for an assumed constant number of waves around the nozzle periphery rather than maximum amplification. Obviously, no definite conclusions are possible concerning the use of integrated growth rates to correlate transition in nozzles until the effects of favorable pressure gradients and axisymmetric geometry can be incorporated in compressible theory. Much more detailed experimental investigations are also required to determine the wave-number criteria that control the formation of the vortices and their subsequent growth. This task would be very difficult, if not impossible, in the present small scale nozzles since the extremely thin boundary layers in the upstream regions of the nozzles are not easily accessible for probing. Meanwhile, it is tentatively concluded that transition can be expected in axisymmetric supersonic nozzles with polished walls when $G \approx 5$ to 6. It should be pointed out, however, that the details of how the Görtler vortices are actually involved in the transition process are not known. On the other hand, the formation and amplification of TS waves is not expected to be an important factor in transition due to the large favorable pressure gradients in both nozzles. For this reason, no analysis of TS amplification in the nozzles has yet been attempted.

The Outlook For Transition Studies in Quiet Nozzles

The noise data presented in figure 5 show that when the nozzle boundary layers are laminar, the rms noise levels are reduced by nearly two orders of magnitude if the nozzle walls are polished, accurately machined, and free of dust deposits. Furthermore, from spectral data given in references 17 and 45

for the present nozzles and in reference 25 for the JPL 20-Inch Tunnel, it is known that the free-stream noise spectra for laminar wall boundary layers contain very little energy above 5 kHz. The length of the test section rhombus ℓ that is exposed to these low noise levels can therefore be used as an indication of the maximum streamwise length of a slender test model that could be used in this type of facility for boundary-layer stability and transition studies under these low-level, low-frequency noise conditions. This test rhombus length is given by

$$\ell_T = x_T - x_R$$

where x_T is the probe location on the nozzle center line where transition was first detected at the acoustic origin for the test values of R_∞ from figures 3(a) and 4(a) and x_R is the location of the upstream tip of the test rhombus from table I. The corresponding free-stream length Reynolds numbers $R_{\ell,T}$ are plotted against R_∞/m in figure 18. Shown for comparison are the mean values and approximate data scatter in the local Reynolds number for transition onset on sharp tip cones in atmospheric flight from reference 12 at $M_e \approx 5.0$. The present nozzle data points are near the lower range of the scatter in flight data so it is perhaps not surprising that transition could not be obtained on test cones in either nozzle with laminar wall boundary layers. (See refs. 8 and 46 for tansition data in the slotted nozzle and conventional nozzle, respectively.) If these small nozzles were to be scaled up by a factor of about 4, the resulting nozzle size would be roughly the same as the JPL 20-Inch Tunnel and if transition occurred at the same relative geometric location on the scaled-up nozzles, the free-stream unit Reynolds numbers for transition would be reduced by a factor of 1/4. The resulting values of R_∞ would be in the range of about 1.5×10^6/m to 4×10^6/m. The data point in figure 18 from the JPL tunnel is near the lower limit of this range in R_∞ but with about the same value of R_ℓ as the small nozzles. This point represents the conditions for which the boundary layer on a flat plate in that tunnel at $M_\infty = 4.5$ and the indicated value of R_ℓ was still laminar with the nozzle-wall boundary layers laminar. While this JPL point is on the high side of the flight transition data correlation, transition was still not observed in the tunnel test even though it might be expected that the stream disturbance levels were in the range of those in ideal flight tests. Thus, we are forced to conclude that in order to obtain sufficiently high Reynolds numbers to get transition on simple test models with laminar boundary layers on the nozzle walls, it will be necessary to increase the corresponding values of ℓ_T significantly. This may be possible since machining and surface imperfections tend to remain at the same absolute values as a nozzle is scaled up whereas the boundary layers will be thicker for the larger nozzles at lower values of R_∞. Another possible approach would be to cool the nozzle wall which would stabilize TS waves and might also stabilize the Görtler vortices but probably to a lesser extent (refs. 44 and 55) than the TS waves. Although reference 55 deals with the effect of wall cooling in compressible flow on cross-flow-induced vortices, the effects on Görtler vortices are probably similar. Again, the practical limitation of wall cooling would be the relative sizes of residual roughness compared with the smaller boundary-layer thicknesses due to cooling.

CONCLUDING REMARKS

The onset of transition in the wall boundary layers of two axisymmetric Mach 5 wind-tunnel nozzles has been measured under conditions of extremely low incident disturbance levels. The aerodynamic design of the two nozzles was quite different. The so-called slotted nozzle has a rapid expansion contour and a boundary-layer bleed slot just upstream of the throat. The other nozzle was of conventional design with a more gradual expansion contour and no bleed slot.

When the nozzle walls were maintained in a polished and clean condition and when the bleed slot control valves were open in the slotted nozzle, transition in both nozzles moved gradually upstream as the test Reynolds number was increased. When transition was some distance downstream of the wall inflection point in the concave wall region, the value of the local Görtler parameter G at transiton varied only from about 5 to 6 for both nozzles, whereas the momentum thickness Reynolds number varied from about 750 to 1050. Thus, it was tentatively concluded that for these conditions, Görtler vortices were involved in the transition process in both nozzles.

Oil flow patterns near the exit of the slotted nozzle indicated that with bleed valves open, the Görtler vortices persisted to the nozzle exit, far downstream of transition onset, over a wide range of test unit Reynolds numbers up to about $2.2 \times 10^7/m$. When the Reynolds number was increased above this value, no evidence of the vortices could be seen. When the bleed valves are closed in this nozzle, the lip of the bleed slot trips the boundary layer and turbulent flow occurs over most of the nozzle length even at the lowest test Reynolds number of $4.5 \times 10^6/m$; again, no evidence of the vortices could be seen. A previous limited oil flow study in the conventional nozzle showed that Görtler vortices were present near the exit when the boundary layer was laminar over the entire nozzle wall.

Results from a recent theoretical investigation of the linear stability and growth of Görtler vortices in supersonic flow were utilized to compute the amplification of the vortices. If the amplification ratio is expressed in the usual form as e^n where n is the integral of the local amplification rate factor over the streamwise distance from the neutral point to transition and if the amplification is assumed to follow the maximum theoretical rate from the two-dimensional theory, then n varied from about 6 to 15 for the slotted nozzle and from about 4.5 to 9 for the conventional nozzle. On the other hand, if the assumption is made that the total number of vortices around the periphery of the nozzle is conserved, an entirely different growth path in the G-wavelength plane is obtained and the value of n decreased from 15 for maximum amplification to 6.7 for one sample case in the slotted nozzle. Thus, no definite conclusions are possible regarding the values of n for transition in supersonic nozzles with Görtler vortices present until more is known about the wave-number behavior at the origin of the vortices and over their growth path in the actual flow. Also, the effects of large favorable pressure gradients and the expanding axisymmetric wall geometry should be included in the linear theory.

A brief review of the use of these nozzles for quiet wind tunnels for transition research wherein the nozzle-wall boundary layers would be laminar shows that transition would have to be delayed considerably over the best obtained so far. In this respect, the performance of the present small-scale versions of the polished conventional nozzle and the slotted nozzle were nearly the same.

Langley Research Center
National Aeronautics and Space Administration
Hampton, VA 23665
May 28, 1981

APPENDIX

VORTICITY AND ACOUSTIC DISTURBANCES EXTERNAL TO LAMINAR BOUNDARY LAYER AT ACOUSTIC ORIGINS

As discussed in the text of this report, the large settling chamber was used with both nozzles for all disturbance measurements reported and used herein. Analysis of hot-wire and pressure-transducer data in this settling chamber (refs. 13, 47, and 48) has shown that the measured levels of $\tilde{u}/\bar{u} \approx 0.2$ to 0.4 percent from the hot-wire data on the center line are primarily acoustic disturbances that originate in the supply pipe and control valve. The pressure fluctuations measured with a transducer mounted flush with the wall vary from $\tilde{p}/\bar{p} \approx 0.002$ to 0.005 percent (ref. 47). The levels for both types of data increase with increasing unit Reynolds number; therefore, the lower values would apply for the conditions where laminar boundary layers were observed over essentially the entire length of the nozzle walls at the lowest unit Reynolds number of 5×10^6/m (fig. 5).

Vorticity

The nozzle contraction would, in general, reduce the streamwise component of the fluctuating velocity according to both theory and experiment if vorticity is the dominant mode (refs. 56 and 57). To provide an estimate of the maximum upper limit of vorticity at the acoustic origins in the free-stream flow, the assumptions will be made that, (1) the rms free-stream vorticity at the acoustic origins is the same as that in the settling chamber and (2) the measured streamwise fluctuating velocity in the chamber consists entirely of vorticity. With these assumptions,

$$\left(\frac{\tilde{u}}{\bar{u}}\right)_a = \frac{\bar{u}_o}{\bar{u}_a}\left(\frac{\tilde{u}}{\bar{u}}\right)_o$$

or in terms of local Mach numbers,

$$\left(\frac{\tilde{u}}{\bar{u}}\right)_a = M_o \sqrt{\frac{\gamma - 1}{2} + \frac{1}{M_a^2}}\left(\frac{\tilde{u}}{\bar{u}}\right)_o \tag{A1}$$

This equation illustrates the well-known result that large reductions in normalized vorticity occur when low Mach number flow in a settling chamber is expanded to supersonic Mach numbers.

APPENDIX

Values of $(\tilde{u}/\bar{u})_a$ computed from equation (A1) are listed in table III for typical center-line probe stations x and acoustic origin locations x_a from figures 3, 4, and 5. (The appropriate values of M_a were obtained from fig. 11.) Thus, even with the overly conservative value of $(\tilde{u}/\bar{u})_o = 0.3$ percent (refs. 13, 47, and 48), the maximum computed streamwise vorticity is only 0.0013 percent which is considered too small in comparison with other disturbances to have any significant effect on transition.

Acoustic Disturbances Propagated From Settling Chamber

Candel (ref. 58) has applied Blokhinstev's energy conservation equation for high-frequency acoustic waves propagating in an irrotational isentropic flow to the downstream propagation of plane waves in a supercritical nozzle. Conservation of acoustic energy flux then requires that

$$\frac{\tilde{p}^2}{\bar{\rho}c}(1 + M)^2 S = \text{Constant} \tag{A2}$$

throughout the nozzle where S is the cross-sectional area of a ray tube. Candel assumes the ray tube is defined by the nozzle boundary when the nozzle area and mean flow vary slowly in the streamwise direction.

For acoustic disturbances at low frequencies, Candel (ref. 58) shows that for the transmission of plane waves of lower frequencies, equation (A2) would overpredict the amplitude of transmitted pressure waves by less than 10 percent provided that the dimensionless frequency

$$\omega_* \geqq \frac{0.8(M - M_o)}{M_o} \tag{A3}$$

where

$$\omega_* = \frac{2\pi f x_o}{c_o}\sqrt{\frac{\gamma + 1}{2}}$$

and x_o is the axial distance from the throat to the nozzle inlet where the transmitted waves enter the nozzle. However, inequality (A3) is based on numerical results for the acoustic admittance in nozzles with inlet Mach numbers of $M_o \geqq 0.13$. Since values of M_o for the conventional and slotted nozzles are about 0.003 and 0.007, respectively, this inequality is not expected to apply very well for these nozzles. A better estimate of the frequency limitations of equation (A2) applied to the present nozzles can be obtained from reference 59 where measurements and theory for the admittances

of a family of nozzles are presented. One of their nozzles had the values of $M_o = 0.08$ and $\theta_w = 45^o$ (in the subsonic approach) which represent the best match to the present conditions. Extrapolation of results from reference 59 to $M_o \approx 0.04$ and results from Candel extrapolated to $M_\infty \approx 5$ then gives a transmission coefficient (ref. 58) for $f > 2000$ Hz that is only 20 percent below the high-frequency ray-tube theory of equation (A2) when applied to the present nozzles. Spectra from hot-wire data in the settling chamber used in the present tests show that significant acoustic energy is present to at least 40 kHz, except at the lowest Reynolds number where the energy is down from the peak levels by about an order of magnitude at 20 kHz. Hence, for the present purpose of estimating a maximum upper limit on noise levels transmitted from the settling chamber, it is concluded that the use of equation (A2) is satisfactory since it will always overpredict the transmitted acoustic energy levels at the lower frequencies.

Candel (ref. 58) also treated the problem of modal propagation (wave motion that has a component perpendicular to the nozzle axis) in nozzles with slowly varying cross-sectional area and mean flow. His results show that for downstream propagation in the subsonic part of the nozzle, the transmission coefficient for a modal disturbance is always greater than for a plane wave propagating in the streamwise direction. On the other hand, if a mode gets through the throat region into the supersonic flow without being cut off, then its transmission coefficient is always less than a plane wave. In conclusion, it may be assumed that for the present purpose, the use of equation (A2) will provide a reasonable estimate of the maximum levels of noise transmitted through a nozzle with slowly varying area and mean flow, even at fairly low frequencies and with some modal type wave motion inclined slightly to the mean flow direction.

However, in the application of equation (A2) to the present nozzles, two basic problems arise: (1) the proper definition and use of the ray-tube area S, particularly for the rapid expansion slotted nozzle and (2) the proper interpretation and use of available pressure-transducer and hot-wire data in both the settling chamber and the supersonic flow. The simplest definition of the ray-tube area for rapid expansion nozzles that seems to be reasonably consistent with the requirements of geometric acoustics is that the area of each individual ray tube remains approximately constant as it passes from the settling chamber through the throat and into the supersonic flow. The ray-tube area may be assumed nearly constant even when the tube is inclined slightly to the nozzle axis. Thus, the predicted intensity of the transmitted noise could be distributed fairly uniformly across the flow at any given nozzle section by, in effect, summing the contribution from all propagating rays including those that may be inclined to the mean flow direction. Without a formal summing procedure, $\tilde{p}^2$ in equation (A2) may then be taken as the total mean square of the propagating noise and S would be assumed constant.

The other problem mentioned above arises from the fact that the input acoustic energy corresponding to the streamwise component of the downstream propagating energy is not available from existing measurements in the settling chamber. Consequently, the constant in equation (A2) cannot be determined with any certainty. Nevertheless, since to first order the hot-wire measures only the streamwise component of the fluctuating velocity, even in low-speed flow

(ref. 13), the resulting mean square velocity is proportional to the streamwise component of the overall acoustic energy flux, including any upstream moving reflected waves, provided only that the acoustic disturbances are much larger than vorticity fluctuations. The fact that, in the present settling chamber, the hot-wire data expressed in terms of pressure fluctuations by the plane wave relation

$$\frac{\tilde{p}}{\bar{p}} = \gamma M \frac{\tilde{u}}{\bar{u}} \tag{A4}$$

are in good agreement with the pressure data measured by a transducer mounted flush with the wall (refs. 13, 47, and 48) is believed to be strong evidence that acoustic waves are the dominant disturbance mode and that the acoustic energy is propagated predominately by plane waves. Of course, these plane waves could be moving both downstream and upstream with some fraction (perhaps small) of the wave motion inclined to the streamwise direction. The conclusion can be made that the mean square of both the hot-wire and pressure-transducer measurements in the settling chamber are roughly proportional to the maximum acoustic energy which could be transmitted downstream. Obviously, comparisons with experimental data are required before either of the two problems (which are (1) use of the ray-tube area S and (2) the fraction of the total measured acoustic energy that is transmitted downstream) can be evaluated as used in equation (A2) for predicting maximum levels of transmitted acoustic energy in wind-tunnel nozzles. These data must be obtained for conditions where all other acoustic disturbances are negligible by comparison with noise transmitted from the settling chamber. These other disturbances include noise radiated from moving eddies in a supersonic transitional or turbulent boundary layer, noise due to shimmering Mach waves, and noise due to any other local sources such as wall slots or holes in transonic tunnels and wall roughness or waviness in supersonic nozzles.

Two situations where these restrictions may be satisfied are (1) the local free-stream Mach number is below about 2.5 where the radiated noise is small (ref. 52) and at the same time any other noise due to local sources is much smaller than the transmitted noise levels or (2) at higher Mach numbers, the boundary layer on the nozzle walls at the acoustic origin locations is laminar with very small oscillations due to instability waves or local wall roughness and waviness. Two sets of data which may qualify under the first category are from references 60 and 61. In both references, data are available for $M_\infty < 2.5$ and the settling chamber noise levels were very high due to the type of pressure control valve used and its location just upstream of the settling chamber inlet diffuser. Consequently, the transmitted noise levels could be large enough to dominate any noise from local sources on the nozzle walls.

Under the second situation noted, some of the present data may qualify. These would be the lowest level data points with $\tilde{p}/\bar{p} < 0.03$ percent for laminar flow in figure 5. The corresponding acoustic origin locations are well upstream such that instability waves may still be small in amplitude. However, as already discussed in the text of this report, the increases in laminar noise

levels for the slotted nozzle from $\tilde{p}/\bar{p} \approx 0.015$ percent at $x \approx 26$ cm to about 0.1 percent for $x \approx 14$ cm as shown in figure 5 for $R_\infty = 5 \times 10^6/m$ are probably caused by shimmering Mach waves induced by increasing wall waviness and the very thin boundary layers for values of $x_a < 8$ cm. (See fig. 13 in ref. 18.) Also, the increases in these low laminar noise levels with increasing R_∞, preceding transition, as seen in figures 3(a) and 4(a) are probably caused primarily by increases in shimmering Mach wave noise due to the decrease in boundary-layer thickness with increasing R_∞.

Before proceeding with the comparisons, equation (A2) is written in terms of the local Mach number by utilizing the equations for isentropic flow from the settling chamber to any downstream point along a streamline. Also, to account for the fact that only part of the total measured acoustic energy in the settling chamber is transmitted through the throat and into the supersonic part of the nozzle, the empirical factor K is introduced into equation (A2) which may then be written as

$$\frac{\tilde{p}^2}{\bar{\rho} c}(1 + M)^2 S = K \frac{\tilde{p}_o{}^2}{(\bar{\rho} c)_o}(1 + M_o)^2 S_o \tag{A5}$$

Thus, if $\tilde{p}_o{}^2$ is taken as the acoustic pressure fluctuations measured in the settling chamber, either with a flush transducer at the wall or a hot wire in the flow, K is the fraction of that energy which is transmitted downstream. Solving for the local normalized rms pressure and noting that $M_o << 1$ then gives the expression

$$\frac{\tilde{p}}{\bar{p}} = \sqrt{K} \frac{\sqrt{M\left(1 + \frac{\gamma - 1}{2} M^2\right)}}{1 + M} \frac{1 + M_o}{\sqrt{M_o}} \left(\frac{\tilde{p}}{\bar{p}}\right)_o \tag{A6}$$

where S is taken as the one-dimensional stream-tube area. If S is assumed constant, in accordance with the concept that some of the very high-frequency acoustic energy could be "beamed" directly through the throat with negligible changes in ray-tube area, equation (A5) becomes

$$\frac{\tilde{p}}{\bar{p}} = \sqrt{K} \frac{\left(1 + \frac{\gamma - 1}{2} M^2\right)^{(3\gamma-1)/4(\gamma-1)}}{1 + M} \left(\frac{\tilde{p}}{\bar{p}}\right)_o \tag{A7}$$

APPENDIX

First, values of $\tilde{p}/\bar{p}$ computed from equation (A7) for $K = 1$ are compared with center-line measurements from figure 5 as given in table III. These computed values (column ⑦) at the acoustic origin Mach numbers are always less than the measured values (column ⑧). This result seems plausible even with the assumption $K = 1$ since the measured center-line values would probably include some shimmering Mach wave noise and may also be subject to axisymmetric focusing effects (ref. 18). It may be tentatively concluded that the minimum values measured on the center line, where $M_\infty = 5.0$, probably include a significant fraction of noise propagated from the settling chamber. Note also that the computed value for $M = 5$ of $\tilde{p}/\bar{p} = 0.012$ percent is close to these minimum measured values. However, the assumption that $K = 1$ is not physically realistic; therefore, the indicated agreement at $M = 5$ is probably influenced by the assumption that $S = \text{Constant}$ used in equation (A7). Furthermore, the lack of any detectable energy in the hot-wire signal at frequencies above 10 kHz when the nozzle-wall boundary layer is laminar (refs. 13 and 16) suggests that the noise propagated from the settling chamber to the Mach 5 flow may be small since the noise in the chamber did contain significant energy up to about 20 kHz even at the lowest Reynolds number. (For $R_\infty = 5 \times 10^6/\text{m}$, the values of unit Reynolds number in the settling chamber were $2.8 \times 10^5/\text{m}$ and $1.2 \times 10^5/\text{m}$ for the slotted and conventional nozzles, respectively.)

To determine if these difficulties can be resolved, data from references 60 and 61 are compared with predictions from both equations (A6) and (A7) in figure 19. Measured values of $(\tilde{p}/\bar{p})_\infty$ are plotted against corresponding values of $(\tilde{p}/\bar{p})_o$ in figure 19(a) for comparison with equation (A7); for comparison with equation (A6), measured values of $(\tilde{p}/\bar{p})_\infty$ are plotted against the quantity $\left[(1 + M_o)/\sqrt{M_o}\right](\tilde{p}/\bar{p})_o$ in figure 19(b). Westley (ref. 60) measured the pressure fluctuations with microphones mounted flush with the wall. The frequency response of the piezoelectric crystals used in the microphones was flat to ±3 dB from 20 Hz to 120 kHz. To obtain the data points shown in figure 19, the mean square of turbulent-boundary-layer wall noise (from ref. 62) has been subtracted from the mean square of the measured noise in the test section since in reference 60 the data were obtained underneath the turbulent boundary layer on the nozzle wall and in reference 61 the data were obtained on a flat plate or cone where the boundary layer was probably turbulent.

The very large noise levels measured in these settling chambers may be compared with the low levels from the present settling chamber in figure 19(a) where some data from figure 5 at $R_\infty = 5 \times 10^6/\text{m}$ are also included. The settling chamber noise levels used for the present data are from the pressure transducer measurements of reference 47. The data of Westley for $M_\infty \leqq 1.96$ group together in bands that follow the predicted trends but are considerably higher than the predicted levels from equation (A7). Thus, even with the assumption of $K = 1$, the use of constant-area ray tubes seems to underpredict the magnitudes of propagated acoustic energy. On the other hand, the agreement of these lower Mach number data with the predicted trends probably indicates the transmitted noise does tend to dominate or overpower any noise from downstream local sources. At $M_\infty = 2.91$, the same effects are apparent but for $(\tilde{p}/\bar{p})_o < 0.5$ percent, the test section levels are nearly constant and much higher than the theory presumably because of the increasing intensity of the noise radiated from the turbulent boundary layers on the nozzle wall

compared with the transmitted noise. At $M_\infty = 3.96$, this local radiated noise completely dominates any transmitted noise.

The use of $K = 0.3$ and the one-dimensional stream-tube area for S in figure 19(b) results in surprisingly good agreement with Westley's data for $M_\infty \leq 1.96$ and also with the lowest levels of the present data for $M_\infty = 5$. From the above discussion, these particular data might be expected to agree best with the noise transmission theory. However, the rather wide range of M_o values and the large differences in settling chamber and nozzle dimensions of the present and Westley's facilities were expected to require different values of K and effective ray-tube areas. Hence, the tendency of the data for low Mach numbers and high noise levels to approach the predictions together with the agreement of the low level Mach 5 data suggests that equation (A6) does indeed provide a good estimate of maximum transmitted noise levels and that roughly 30 percent of the noise energy measured in the settling chamber of typical wind tunnels is propagated into the supersonic flow. It may be concluded that when the rms acoustic disturbances, $(\tilde{p}/\bar{p})_o > 0.5$ percent and when $M_\infty < 3$, noise transmitted from the settling chamber will dominate noise from downstream local sources. For conditions of the present tests it seems reasonably certain that for typical acoustic origin Mach numbers ($M_a < 4$), the transmitted noise at the lowest unit Reynolds numbers is less than 0.01 percent. At higher unit Reynolds numbers, transition moves upstream into the nozzles (fig. 6), and the local transmitted noise levels would increase but only in proportion to $(\tilde{p}/\bar{p})_o$ which increases roughly by a factor of 2 from the lowest to the highest values of R_∞ (refs. 13 and 48).

Shimmering Mach Wave Noise

In supersonic flow, the Mach lines caused by wall roughness or waviness oscillate or shimmer at high frequencies when the wall boundary layer is turbulent. This type of noise has been detected with hot-wire techniques (refs. 18 and 63) which show that the slope of the mode plot line increases but the intercept remains fixed when shimmering Mach wave noise is present. When the wall boundary layer is laminar, the Mach lines caused by wall imperfections may also shimmer and the hot-wire mode plot reveals this noise mechanism by an increase in slope of the lines but with zero intercept which indicates the source is stationary. In this case, the Mach waves shimmer at smaller frequencies, usually less than 5 kHz due to any unsteadiness or instability waves in the laminar boundary layer (ref. 13). Presumably, any unsteadiness in the free stream could also shimmer the Mach waves but this effect is probably small as indicated by the apparent absence of high-frequency energy in the hot-wire signal. As mentioned previously, this lack of high-frequency energy in the hot-wire signal when the nozzle-wall boundary layer is laminar also suggests that noise propagation from the settling chamber into the Mach 5 flow may not be a dominant factor in the total noise levels since the acoustic disturbances in the settling chamber certainly contained energy above 5 kHz even at the lowest Reynolds number (ref. 13). In any case, when the boundary layer is laminar, it is clear the amplitude of the shimmering Mach wave noise is determined primarily by the distribution and magnitude of local wall imperfections and the boundary-layer thickness. Thus, from the laminar data in figure 5 for

the conventional nozzle, the rough wall data is more than three times higher than the polished wall data at $x = 37.5$ cm.

For the slotted nozzle, those measured center-line values in figure 5 that are above 0.03 percent are clearly due to shimmering Mach waves probably caused by axisymmetric wall waviness (ref. 18) and, therefore, subject to strong axisymmetric focusing on the nozzle center line. As mentioned previously, the large increases of up to about an order of magnitude in center-line noise with increasing unit Reynolds number when the boundary layer at the acoustic origins is still laminar (figs. 3(a) and 4(a)), may also be attributed to increases in shimmering Mach wave noise as the boundary layer becomes thinner. Some of this increase on the center line can be attributed to strong focusing effects, so increases in local levels with increasing R_∞ may be about 1/2 order of magnitude. The local free-stream pressure fluctuations at the acoustic origins due to shimmering waves which originate even further upstream cannot be determined without local measurements near the boundary-layer edge. Since the shimmering waves appear to cause mainly low-frequency noise, they may not be critically involved anyway in the boundary-layer instability and transition process which is sensitive to high-frequency disturbances. Indeed, the rather uniform upstream movement of transition with increasing R_∞ as shown in figure 6 may be taken as evidence that possible abrupt spatial changes in local shimmering Mach wave noise have not affected transition, although the increases in this noise with increasing unit Reynolds number may be involved. Thus, while some uncertainty remains concerning the local levels of shimmering Mach wave noise, it seems likely that these levels would not exceed the minimum measured center-line values which would generally be larger than incident local levels due to axisymmetric focusing effects. Hence, it may be concluded that free-stream levels of shimmering Mach wave noise incident upon the laminar boundary layer at low Reynolds numbers are less than 0.01 percent. At higher Reynolds numbers, the local shimmering Mach wave noise may increase to the order of 0.05 percent.

In conclusion, it seems clear that the minimum center-line noise levels measured in the present nozzles ($(\tilde{p}/\bar{p})_\infty < 0.03$ percent) consist of both shimmering Mach wave noise and noise transmitted from the settling chamber. The good agreement between the qualifying experimental data over the Mach number range from 1.2 to 5 as shown in figure 19(b) suggests that the transmitted noise may dominate, whereas at $M_\infty = 5$ the apparent lack of high-frequency energy in the hot-wire signal and the mode plot evidence of fixed sources favor the shimmering Mach wave sources. Obviously, the relative contributions from these two entirely different sources cannot be determined without more detailed measurements including spectral data and cross-correlation data for two probes.

REFERENCES

1. Pate, S. R.; and Schueler, C. J.: Radiated Aerodynamic Noise Effects on Boundary-Layer Transition in Supersonic and Hypersonic Wind Tunnels. AIAA J., vol. 7, no. 3, Mar. 1969, pp. 450-457.

2. Wagner, R. D., Jr.; Maddalon, D. V.; and Weinstein, L. M.: Influence of Measured Freestream Disturbances on Hypersonic Boundary-Layer Transition. AIAA J., vol. 8, no. 9, Sept. 1970, pp. 1664-1670.

3. Pate, S. R.: Measurements and Correlations of Transition Reynolds Numbers on Sharp Slender Cones at High Speeds. AIAA J., vol. 9, no. 6, June 1971, pp. 1082-1090.

4. Stainback, P. Calvin: Hypersonic Boundary-Layer Transition in the Presence of Wind-Tunnel Noise. AIAA J., vol. 9, no. 12, Dec. 1971, pp. 2475-2476.

5. Stainback, P. C.; Fischer, M. C.; and Wagner, R. D.: Effects of Wind-Tunnel Disturbances on Hypersonic Boundary-Layer Transition. Parts I and II. AIAA Paper No. 72-181, Jan. 1972.

6. Dougherty, N. S., Jr.: Correlation of Transition Reynolds Number With Aerodynamic Noise Levels in a Wind Tunnel at Mach Numbers 2.0-3.0. AIAA J., vol. 13, no. 12, Dec. 1975, pp. 1670-1671.

7. Anders, J. B.; Stainback, P. C.; Keefe, L. R.; and Beckwith, I. E.: Fluctuating Disturbances in a Mach 5 Wind Tunnel. AIAA J., vol. 15, no. 8, Aug. 1977, pp. 1123-1129.

8. Trimpi, Robert L.: Modern Fluid Dynamics of Supersonic and Hypersonic Flight. AIAA-80-0862, May 1980.

9. Kendall, J. M.: Wind Tunnel Experiments Relating to Supersonic and Hypersonic Boundary-Layer Transition. AIAA J., vol. 13, no. 3, Mar. 1975, pp. 290-299.

10. Mack, Leslie M.: Linear Stability Theory and the Problem of Supersonic Boundary-Layer Transition. AIAA J., vol. 13, no. 3, Mar. 1975, pp. 278-289.

11. Dougherty, N. S., Jr.; and Fisher, D. F.: Boundary-Layer Transition on a 10 Deg Cone: Wind Tunnel/Flight Correlation. AIAA-80-0154, Jan. 1980.

12. Beckwith, I. E.: Development of a High Reynolds Number Quiet Tunnel for Transition Research. AIAA J., vol. 13, no. 3, Mar. 1975, pp. 300-306.

13. Anders, J. B.; Stainback, P. C.; Keefe, L. R.; and Beckwith, I. E.: Fluctuating Disturbances in a Mach 5 Wind Tunnel. Proceedings - AIAA 9th Aerodynamic Testing Conference, June 1976, pp. 185-197.

14. Beckwith, I. E.; Anders, J. B.; Stainback, P. C.; Harvey, W. D.; and Srokowski, A. J.: Progress in the Development of a Mach 5 Quiet Tunnel. Laminar-Turbulent Transition, AGARD-CPP-224, May 1977, pp. 28-1 - 28-14.

15. Beckwith, Ivan E.; Harvey, William D.; Harris, Julius E.; and Holley, Barbara B.: Control of Supersonic Wind-Tunnel Noise by Laminarization of Nozzle-Wall Boundary Layers. NASA TM X-2879, 1973.

16. Harvey, William D.; Cary, Aubrey M., Jr.; and Harris, Julius E.: Experimental and Numerical Investigation of Boundary-Layer Development and Transition on the Walls of a Mach 5 Nozzle. NASA TN D-7976, 1975.

17. Harvey, W. D.; Stainback, P. C.; Anders, J. B.; and Cary, A. M.: Nozzle Wall Boundary-Layer Transition and Freestream Disturbances at Mach 5. AIAA J., vol. 13, no. 3, Mar. 1975, pp. 307-314.

18. Anders, J. B.; Stainback, P. C.; and Beckwith, I. E.: A New Technique for Reducing Test Section Noise in Supersonic Wind Tunnels. A Collection of Technical Papers - AIAA 10th Aerodynamic Testing Conference, Apr. 1978, pp. 354-364. (Available as AIAA Paper 78-817.)

19. Smith, A. M. O.: On the Growth of Taylor-Görtler Vortices Along Highly Concave Walls. Q. Appl. Math., vol. XIII, no. 3, Oct. 1955, pp. 233-262.

20. Jaffe, N. A.; Okamura, T. T.; and Smith, A. M. O.: Determination of Spatial Amplification Factors and Their Application to Predicting Transition. AIAA J. vol. 8, no. 2, Feb. 1970, pp. 301-308.

21. Mack, Leslie M.: A Numerical Method for the Prediction of High-Speed Boundary-Layer Transition Using Linear Theory. Aerodynamic Analyses Requiring Advanced Computers - Part I, NASA SP-347, 1975, pp. 101-123.

22. Mack, Leslie M.: Transition Prediction and Linear Stability Theory. Laminar-Turbulent Transition, AGARD-CP-224, Oct. 1977, pp. 1-1 - 1-22.

23. Runyan, L. James; and George-Falvy, Dezso: Amplification Factors at Transition on an Unswept Wing in Free Flight on a Swept Wing in Wind Tunnel. AIAA Paper 79-0267, Jan. 1979.

24. Smith, A. M. O.; and Gamberoni, Nathalie: Transition, Pressure Gradient, and Stability Theory. Rep. No. ES 26388, Douglas Aircraft Co., Inc., Aug. 31, 1956. (Also available in IX Congrès International de Mécanique Appliquée, Tome IV, Université de Bruxelles, 1957, pp. 234-244.)

25. Morkovin, Mark V.: Critical Evaluation of Transition From Laminar to Turbulent Shear Layers with Emphasis on Hypersonically Traveling Bodies. AFFDL-TR-68-149, U.S. Air Force, Mar. 1969. (Available from DTIC as AD 686 178.)

26. Gregory, N.; Stuart, J. T.; and Walker, W. S.: On the Stability of Three-Dimensional Boundary Layers With Applications to the Flow Due to a Rotating Disk. Philos. Trans. R. Soc. London, Ser. A, vol. 248, no. 943, July 14, 1955, pp. 155-199.

27. Owen, P. R.; and Randall, D. G.: Boundary Layer Transition on a Sweptback Wing: Effect of Incidence. Tech. Memo. No. Aero.375, British R.A.E., Oct. 1953.

28. Beckwith, Ivan E.; and Gallagher, James J.: Experimental Investigation of the Effect of Boundary-Layer Transition on the Average Heat Transfer to a Yawed Cylinder in Supersonic Flow. NACA RM L56E09, 1956.

29. Chapman, Gary T.: Some Effects of Leading-Edge Sweep on Boundary-Layer Transition at Supersonic Speeds. NASA TN D-1075, 1961.

30. Srokowski, Andrew J.; and Orszag, Steven A.: Mass Flow Requirements for LFC Wing Design. AIAA Paper 77-1222, Aug. 1977.

31. Mack, Leslie M.: On the Stability of the Boundary Layer on a Transonic Swept Wing. AIAA Paper 79-0264, Jan. 1979.

32. Nayfeh, Ali H.: Stability of Three-Dimensional Boundary Layers. AIAA Paper 79-0262, Jan. 1979.

33. Hefner, Jerry N.; and Bushnell, Dennis M.: Status of Linear Boundary-Layer Stability Theory and the e^n Method, With Emphasis on Swept-Wing Applications. NASA TP-1645, 1980.

34. Görtler, H.: On the Three-Dimensional Instability of Laminar Boundary Layers on Concave Walls. NACA TM 1375, 1954. (Translation of "Über eine dreidimensionale Instabilität laminarer Grenzschichten an konkaven Wänden, Ges. d. Wiss, Göttingen, Nachr. a. d. Math., Bd. 2, Nr. 1, 1940.)

35. Gregory, N.; and Walker, W. S.: Part I - The Effect on Transition of Isolated Surface Excrescences in the Boundary Layer. R. & M. No. 2779, British A.R.C., 1956.

36. Liepmann, H. W.: Investigation of Boundary Layer Transition on Concave Walls. NACA WR W-87, 1945. (Formerly NACA ACR 4J28.)

37. Schlichting, Hermann (J. Kestin, transl.): Boundary-Layer Theory, Sixth ed. McGraw-Hill Book Co., Inc., c.1968.

38. Tani, Itiro; and Aihara, Yasuhiko: Görtler Vortices and Boundary-Layer Transition. Z. Angew. Math. Phys., vol. 20, Sept. 25, 1969, pp. 609-618.

39. Nayfeh, Ali H.: Effect of Streamwise Vortices on Tollmien-Schlichting Waves. VPI-E-79.12, Virginia Polytech. Inst. & State Univ., Mar. 1979. (Available as NASA CR-162654.)

40. Nayfeh, Ali Hasan: Perturbation Methods, John Wiley & Sons, Inc., c.1973, ch. 6.

41. Floryan, Jerzy M.; and Saric, William S.: Stability of Görtler Vortices in Boundary Layers With Suction. AIAA Paper 79-1497, July 1979.

42. Floryan, Jerzy M.; and Saric, William S.: Wavelength Selection and Growth of Görtler Vortices. AIAA-80-1376, July 1980.

43. Ragab, S. A.; and Nayfeh, A. H.: Effect of Pressure Gradients on Görtler Instability. AIAA-80-1377, July 1980.

44. Kobayashi, Ryoji; and Kohama, Yasuaki: Taylor-Görtler Instability of Compressible Boundary Layers. AIAA J., vol. 15, no. 12, Dec. 1977, pp. 1723-1727.

45. Stainback, P. C.; Anders, J. B.; Harvey, W. D.; Cary, A. M.; and Harris, J. E.: An Investigation of Boundary-Layer Transition on the Wall of a Mach 5 Nozzle. AIAA Paper No. 74-136, Jan.-Feb. 1974.

46. Stainback, P. C.; and Wagner, R. D.: A Comparison of Disturbance Levels Measured in Hypersonic Tunnels Using a Hot-Wire Anemometer and a Pitot Pressure Probe. AIAA Paper No. 72-1003, Sept. 1972.

47. Anders, J. B.; Stainback, P. C.; Keefe, L. R.; and Beckwith, I. E.: Sound and Fluctuating Disturbance Measurements in the Settling Chamber and Test Section of a Small, Mach 5 Wind Tunnel. ICIASF '75 Record, IEEE Publ. 75 CHO 993-6 AES, Sept. 1975, pp. 329-340.

48. Beckwith, I. E.: Comments on Settling Chamber Design for Quiet, Blowdown Wind Tunnels. NASA TM-81948, 1981.

49. Hopkins, D. F.; and Hill, D. E.: Effect of Small Radius of Curvature on Transonic Flow in Axisymmetric Nozzles. AIAA J., vol. 4, no. 8, Aug. 1966, pp. 1337-1343.

50. Price, Joseph M.; and Harris, Julius E.: Computer Program for Solving Compressible Nonsimilar-Boundary-Layer Equations for Laminar, Transitional, or Turbulent Flows of a Perfect Gas. NASA TM X-2458, 1972.

51. The Magic of Day-Glow Fluorescent Pigments. Tech. Bull. No. 1206, Day-Glo Color Corp., 1977.

52. Laufer, John: Some Statistical Properties of the Pressure Field Radiated by a Turbulent Boundary Layer. Phys. Fluids, vol. 7, no. 8, Aug. 1964, pp. 1191-1197.

53. Rotta, J. C.: Effect of Streamwise Wall Curvature on Compressible Turbulent Boundary Layers. Phys. Fluids Suppl., vol. 10, pt. II, no. 9, Sept. 1967, pp. S174-S180.

54. Pfenninger, W.; and Syberg, J.: Reduction of Acoustic Disturbances in the Test Section of Supersonic Wind Tunnels by Laminarizing Their Nozzles and Test Section Wall Boundary Layers by Means of Suction. NASA CR-2436, 1974.

55. Lekoudis, Spyridon: The Stability of the Boundary Layer on a Swept Wing With Wall Cooling. AIAA Paper 79-1495, July 1979.

56. Ribner, H. S.; and Tucker, M.: Spectrum of Turbulence in a Contracting Stream. NACA Rep. 1113, 1953.

57. Beckwith, I. E.; and Rotta, J. C.: Appendix 7 - Effects of Contractions on Turbulence in the Working Section. A Further Review of Current Research Aimed at the Design and Operation of Large Wind Tunnels. AGARD-AR-83, Sept. 1975, pp. 113-117.

58. Candel, S. M.: Acoustic Conservation Principles and an Application to Plane and Modal Propagation in Nozzles and Diffusers. J. Sound & Vib., vol. 41, no. 2, July 22, 1975, pp. 207-232.

59. Bell, W. A.; Daniel, B. R.; and Zinn, B. T.: Experimental and Theoretical Determination of the Admittances of a Family of Nozzles Subjected to Axial Instabilities. J. Sound & Vib., vol. 30, no. 2, 1973, pp. 179-190.

60. Westley, R.: Aerodynamic Sound and Pressure Fluctuations in a Supersonic Blowdown Wind Tunnel. Aeronaut. Rep. LR-274 (N.R.C. No. 5916), Jan. 1960.

61. Cooksey, James M.; and Arnold, John W.: Transonic Flow Quality Improvements in a Blowdown Wind Tunnel. J. Aircr., vol. 10, no. 9, Sept. 1973, pp. 554-560.

62. Harvey, William D.; Bushnell, Dennis M.; and Beckwith, Ivan E.: Fluctuating Properties of Turbulent Boundary Layers for Mach Numbers up to 9. NASA TN D-5496, 1969.

63. Laufer, John: Aerodynamic Noise in Supersonic Wind Tunnels. J. Aerosp. Sci., vol. 28, no. 9, Sept. 1961, pp. 685-692.

TABLE I.- NOZZLE DIMENSIONS

	Slotted nozzle	Conventional nozzle
Throat radius, r_*, cm	1.272	1.005
Exit radius, r_E, cm	6.455	5.340
Length from throat to exit, L, cm	39.307	50.002
Maximum wall angle at inflection point, deg	22.64	10.37
Axial distance from throat to -		
Slot lip, cm	-1.143	------
Inflection point (G = 0), cm	1.359	8.832
Upstream tip of test rhombus, x_R, cm	13.74	23.32

TABLE II.- SMOOTHED DESIGN COORDINATES FOR SLOTTED NOZZLE

(a) Subsonic approach and outer wall of slot

x		r		M_e	x		r		M_e
in.	cm	in.	cm		in.	cm	in.	cm	
-10.939	-27.785	5.750	14.605	0.007	-2.439	-6.195	2.843	7.221	0.027
-10.700	-27.178	5.745	14.591		-2.189	-5.560	2.616	6.645	.032
-10.450	-26.543	5.734	14.564		-1.939	-4.925	2.385	6.058	.038
-10.200	-25.908	5.720	14.528		-1.689	-4.290	2.150	5.461	.047
-9.950	-25.273	5.700	14.477		-1.439	-3.655	1.914	4.862	.057
-9.700	-24.638	5.677	14.418		-1.189	-3.020	1.675	4.255	.069
-9.450	-24.003	5.652	14.356		-.939	-2.385	1.428	3.627	.087
-9.200	-23.368	5.627	14.291		-.839	-2.131	1.324	3.363	.099
-8.950	-22.733	5.601	14.227		-.819	-2.080	1.303	3.310	.103
-8.700	-22.098	5.573	14.155		-.760	-1.930	1.238	3.145	.114
-8.450	-21.463	5.545	14.083		-.680	-1.727	1.147	2.913	.132
-8.200	-20.828	5.515	14.008		-.595	-1.511	1.043	2.649	.158
-7.950	-20.193	5.485	13.931		-.536	-1.361	.965	2.451	.192
-7.700	-19.558	5.454	13.853		-.491	-1.247	.905	2.299	.226
-7.450	-18.923	5.424	13.777		-.454	-1.153	.856	2.174	.261
-7.200	-18.288	5.394	13.700		-.424	-1.077	.819	2.080	.296
-6.950	-17.653	5.362	13.620	.008	-.394	-1.001	.786	1.996	.330
-6.700	-17.018	5.328	13.532		-.379	-.963	.771	1.958	.60
-6.450	-16.383	5.291	13.438		-.360	-.914	.754	1.915	.72
-6.200	-15.748	5.248	13.330		-.344	-.874	.743	1.887	.80
-5.950	-15.113	5.199	13.210		-.323	-.820	.732	1.859	.90
-5.700	-14.478	5.138	13.051		-.302	-.767	.724	1.839	1.15
-5.450	-13.843	5.055	12.838	.009	-.279	-.709	.720	1.829	1.29
-5.200	-13.208	4.941	12.549		-.252	-.640	.728	1.849	
-4.950	-12.573	4.816	12.233		-.224	-.569	.750	1.905	
-4.700	-11.938	4.669	11.859	.010	-.205	-.521	.776	1.971	
-4.450	-11.303	4.497	11.421	.011	-.194	-.493	.795	2.019	
-4.200	-10.668	4.310	10.946	.012	-.187	-.475	.813	2.065	
-4.189	-10.640	4.302	10.926	.012	-.182	-.462	.830	2.108	
-3.939	-10.005	4.108	10.434	.013	-.178	-.452	.850	2.159	
-3.689	-9.370	3.913	9.939	.014	-.176	-.447	.865	2.197	
-3.439	-8.735	3.711	9.425	.016	-.174	-.442	.900	2.286	
-3.189	-8.100	3.502	8.895	.018	-.172	-.437	.940	2.388	
-2.939	-7.465	3.286	8.346	.020	-.172	-.437	1.075	2.731	
-2.689	-6.830	3.068	7.793	.023					

TABLE II.- Continued

(b) Inner wall of slot

x		r		M_e
in.	cm	in.	cm	
[a]-0.434	-1.103	0.682	1.732	
[b]-.431	-1.095	.688	1.748	0.62
-.420	-1.067	.682	1.733	.66
-.400	-1.016	.671	1.705	.75
-.360	-.914	.651	1.654	.90
-.320	-.813	.633	1.608	1.03
-.280	-.711	.618	1.569	1.16
-.240	-.610	.604	1.534	
-.200	-.508	.592	1.504	
-.160	-.406	.582	1.478	
-.120	-.305	.576	1.462	
-.080	-.203	.573	1.456	
-.040	-.102	.575	1.46	
.000	.000	.580	1.473	
.040	.102	.591	1.501	
.080	.203	.606	1.539	
.120	.305	.625	1.588	
.160	.406	.648	1.646	
.200	.508	.676	1.717	
.250	.635	.719	1.826	
.300	.762	.777	1.974	
.350	.889	.859	2.182	
.400	1.016	.975	2.477	
.450	1.143	1.140	2.897	
.500	1.270	1.500	3.810	

[a]Center of leading-edge radius.
[b]Tangent to leading-edge radius.

TABLE II.- Continued

(c) Transonic and supersonic wall

x		r		M_e	x		r		M_e
in.	cm	in.	cm		in.	cm	in.	cm	
[a]-0.4343	-1.1031	0.6820	1.7323		-0.1750	-0.4445	0.5283	1.3419	0.773
[b]-.4388	-1.1146	.6769	1.7193		-.1662	-.4221	.5256	1.3350	.791
-.4276	-1.0861	.6676	1.6957	0.365	-.1576	-.4003	.5231	1.3287	.810
-.4133	-1.0498	.6561	1.6665	.383	-.1490	-.3785	.5207	1.3226	.829
-.3990	-1.0135	.6452	1.6388	.399	-.1405	-.3569	.5185	1.3170	.849
-.3857	-.9797	.6354	1.6139	.417	-.1321	-.3355	.5164	1.3117	.868
-.3725	-.9462	.6262	1.5905	.434	-.1238	-.3145	.5145	1.3068	.888
-.3600	-.9144	.6177	1.5690	.452	-.1156	-.2936	.5127	1.3023	.908
-.3476	-.8829	.6097	1.5486	.469	-.1075	-.2731	.5111	1.2982	.928
-.3358	-.8529	.6024	1.5301	.486	-.0994	-.2525	.5096	1.2944	.948
-.3241	-.8232	.5954	1.5123	.503	-.0914	-.2322	.5082	1.2908	.969
-.3129	-.7948	.5889	1.4958	.521	-.0835	-.2121	.5069	1.2875	.989
-.3017	-.7663	.5827	1.4801	.538	-.0756	-.1920	.5058	1.2847	1.011
-.2909	-.7389	.5770	1.4656	.556	-.0678	-.1722	.5048	1.2822	1.032
-.2802	-.7117	.5715	1.4516	.573	-.0601	-.1527	.5039	1.2799	1.053
-.2699	-.6855	.5664	1.4387	.591	-.0524	-.1331	.5031	1.2779	1.075
-.2597	-.6596	.5615	1.4262	.608	-.0470	-.1194	.5024	1.2761	1.091
-.2498	-.6345	.5569	1.4145	.626	-.0371	-.0942	.5018	1.2746	1.120
-.2398	-.6091	.5525	1.4034	.644	-.0296	-.0752	.5013	1.2733	1.142
-.2302	-.5847	.5485	1.3932	.662	-.0221	-.0561	.5010	1.2725	1.165
-.2206	-.5603	.5446	1.3833	.680	-.0147	-.0373	.5008	1.2720	1.189
-.2113	-.5367	.5409	1.3739	.698	-.0073	-.0185	.5006	1.2715	1.212
-.2020	-.5131	.5375	1.3653	.717	.0000	.0000	.5005	1.2713	1.236
-.1929	-.4900	.5342	1.3569	.735	.0074	.0188	.5006	1.2715	1.261
-.1839	-.4671	.5312	1.3492	.754	.0147	.0373	.5008	1.2720	1.286

[a]Center of leading-edge radius.
[b]Tangent to leading-edge radius.

TABLE II.- Continued

(c) Continued

x		r		M_e	x		r		M_e
in.	cm	in.	cm		in.	cm	in.	cm	
0.0219	0.0556	0.5010	1.2725	1.311	0.3200	0.8128	0.5887	1.4953	2.048
.0291	.0739	.5014	1.2736	1.337	.3413	.8669	.5972	1.5169	2.071
.0362	.0919	.5019	1.2748	1.363	.3648	.9266	.6068	1.5413	2.095
.0434	.1102	.5024	1.2761	1.390	.3883	.9863	.6164	1.5657	2.118
.0505	.1283	.5031	1.2779	1.417	.4139	1.0513	.6270	1.5926	2.142
.0575	.1461	.5038	1.2797	1.438	.4394	1.1161	.6375	1.6193	2.167
.0644	.1636	.5047	1.2819	1.459	.4673	1.1869	.6492	1.6490	2.192
.0715	.1816	.5057	1.2845	1.494	.4951	1.2576	.6608	1.6784	2.218
.0786	.1996	.5069	1.2875	1.532	.5255	1.3348	.6736	1.7109	2.245
.0856	.2174	.5081	1.2906	1.561	.5559	1.4120	.6863	1.7432	2.272
.0925	.2350	.5094	1.2939	1.591	.5885	1.4948	.6999	1.7777	2.295
.1063	.2700	.5124	1.3015	1.654	.6210	1.5773	.7135	1.8123	2.327
.1200	.3048	.5159	1.3104	1.722	.6556	1.6652	.7279	1.8489	2.354
.1336	.3393	.5198	1.3203	1.789	.6902	1.7531	.7423	1.8854	2.383
.1479	.3757	.5239	1.3307	-----	.7265	1.8453	.7573	1.9235	2.410
[c].1614	.4100	.5285	1.3424	-----	.7628	1.9375	.7722	1.9614	2.438
.1756	.4460	.5333	1.3546	1.867	.8009	2.0343	.7878	2.0010	2.465
.1876	.4765	.5376	1.3655	1.885	.8389	2.1309	.8033	2.0404	2.493
.1996	.5070	.5419	1.3764	1.903	.8784	2.2311	.8193	2.0810	2.520
.2138	.5431	.5472	1.3899	1.921	.9179	2.3315	.8352	2.1214	2.548
.2278	.5786	.5526	1.4036	1.941	.9588	2.4354	.8516	2.1631	2.574
.2444	.6208	.5589	1.4196	1.960	.9996	2.5390	.8678	2.2042	2.602
.2609	.6627	.5653	1.4359	1.981	1.0858	2.7579	.9017	2.2903	2.651
.2798	.7107	.5727	1.4547	2.003	1.1720	2.9769	.9349	2.3746	2.706
.2986	.7584	.5802	1.4737	2.025	1.2630	3.2080	.9694	2.4623	2.756

[c]Method of characteristics starts.

TABLE II.- Continued

(c) Continued

x		r		M_e	x		r		M_e
in.	cm	in.	cm		in.	cm	in.	cm	
1.3540	3.4392	1.0030	2.5476	2.811	4.4735	11.3627	1.8107	4.5992	3.885
1.4505	3.6843	1.0379	2.6363	2.861	4.6290	11.7577	1.8382	4.6690	3.921
1.5470	3.9298	1.0719	2.7226	2.916	4.7870	12.1590	1.8653	4.7379	3.953
1.6490	4.1885	1.1069	2.8115	2.964	4.9450	12.5603	1.8915	4.8044	3.987
1.7510	4.4475	1.1411	2.8984	3.016	5.1085	12.9756	1.9177	4.8710	4.019
1.8580	4.7193	1.1761	2.9873	3.062	5.2720	13.3909	1.9430	4.9352	4.053
1.9650	4.9911	1.2102	3.0739	3.112	5.4415	13.8214	1.9684	4.9997	4.083
2.0765	5.2743	1.2449	3.1620	3.157	5.6110	14.2519	1.9928	5.0617	4.115
2.1880	5.5575	1.2787	3.2479	3.206	5.7815	14.6850	2.0166	5.1222	4.144
2.3040	5.8522	1.3130	3.3350	3.249	5.9520	15.1181	2.0396	5.1806	4.175
2.4200	6.1468	1.3463	3.4196	3.296	6.1310	15.5727	2.0628	5.2395	4.204
2.5410	6.4541	1.3802	3.5057	3.338	6.3100	16.0274	2.0852	5.2964	4.235
2.6620	6.7615	1.4130	3.5890	3.383	6.4890	16.4821	2.1068	5.3513	4.262
2.7880	7.0815	1.4462	3.6733	3.424	6.6680	16.9367	2.1276	5.4041	4.289
2.9140	7.4016	1.4785	3.7554	3.468	6.8565	17.4155	2.1487	5.4577	4.317
3.0450	7.7343	1.5110	3.8379	3.508	7.0450	17.8943	2.1689	5.5090	4.345
3.1760	8.0670	1.5425	3.9180	3.549	7.2320	18.3693	2.1882	5.5580	4.370
3.3120	8.4125	1.5743	3.9987	3.588	7.4190	18.8443	2.2067	5.6050	4.396
3.4480	8.7579	1.6051	4.0770	3.629	7.6155	19.3434	2.2255	5.6527	4.421
3.5890	9.1161	1.6361	4.1557	3.666	7.8120	19.8425	2.2434	5.6982	4.447
3.7300	9.4742	1.6662	4.2321	3.706	8.0075	20.3391	2.2605	5.7417	4.470
3.8745	9.8412	1.6961	4.3081	3.742	8.2030	20.8356	2.2768	5.7831	4.494
4.0190	10.2083	1.7251	4.3818	3.780	8.4075	21.3551	2.2932	5.8247	4.518
4.1685	10.5880	1.7542	4.4557	3.814	8.6120	21.8745	2.3088	5.8644	4.542
4.3180	10.9677	1.7823	4.5270	3.851	8.8155	22.3914	2.3237	5.9022	4.563

TABLE II.- Concluded

(c) Concluded

x		r		M_e	x		r		M_e
in.	cm	in.	cm		in.	cm	in.	cm	
9.019	22.908	2.3379	5.9383	4.585	12.342	31.347	2.4911	6.3274	4.850
9.233	23.451	2.3521	5.9743	4.606	12.575	31.941	2.4972	6.3429	4.863
9.446	23.993	2.3655	6.0084	4.628	12.811	32.539	2.5029	6.3574	4.877
9.659	24.534	2.3784	6.0411	4.647	13.046	33.137	2.5081	6.3706	4.890
9.872	25.075	2.3905	6.0719	4.668	13.286	33.745	2.5130	6.3830	4.900
10.087	25.621	2.4022	6.1016	4.685	13.525	34.354	2.5174	6.3942	4.910
10.302	26.167	2.4133	6.1298	4.703	13.766	34.966	2.5215	6.4046	4.920
10.523	26.727	2.4240	6.1570	4.722	14.007	35.578	2.5251	6.4138	4.931
10.743	27.287	2.4341	6.1826	4.741	14.250	36.195	2.5285	6.4224	4.941
10.968	27.857	2.4438	6.2073	4.757	14.493	36.812	2.5316	6.4303	4.952
11.192	28.428	2.4530	6.2306	4.774	14.738	37.433	2.5343	6.4371	4.958
11.419	29.003	2.4616	6.2525	4.791	14.982	38.054	2.5369	6.4437	4.965
11.645	29.578	2.4696	6.2728	4.809	15.229	38.680	2.5392	6.4496	4.971
11.877	30.166	2.4773	6.2923	4.823	15.475	39.307	2.5413	6.4549	4.978
12.108	30.754	2.4844	6.3104	4.837					

TABLE III.- ESTIMATED MAXIMUM LEVELS OF VORTICITY AND NOISE AT ACOUSTIC ORIGINS

①	②	③	④	⑤	⑥	⑦	⑧
Nozzle	x/L	x, cm	x_a, cm	M_a	$(\tilde{u}/\bar{u})_a$, percent (a)	$\tilde{p}/\bar{p}$, percent (b)	$\tilde{p}/\bar{p}$, percent (c)
Conventional	0.441	22.0	9.5	3.11	0.0012	0.0042	0.071
	.594	29.7	12.5	3.56	.0011	.0055	.078
	.750	37.5	18.2	4.11	.0011	.0075	.025
Slotted	0.321	12.6	1.1	2.18	0.0013	0.0024	0.062
	.435	17.1	2.2	2.52	.0013	.0063	.074
	.677	26.6	6.0	3.26	.0011	.0046	.013
Test section	Any location			5.0	0.0010	0.0120	

[a]Computed from equation (A1) with $M_o = 0.007$ and $(\tilde{u}/\bar{u})_o = 0.003$.
[b]Computed from equation (A7).
[c]Experimental values on the center line from figure 5 at $R_\infty = 5 \times 10^6/m$.

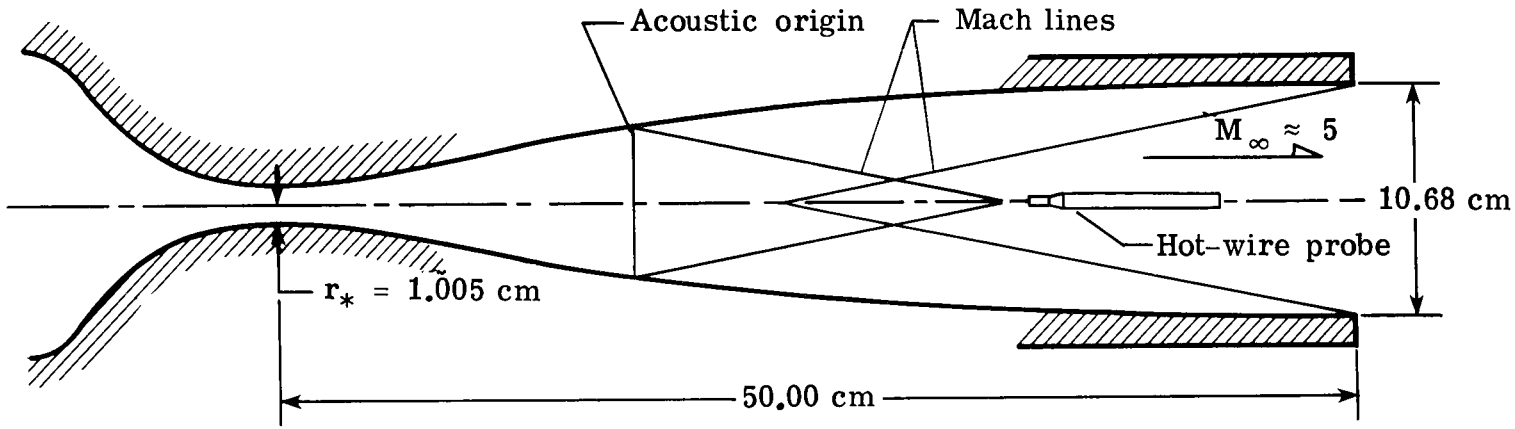

Conventional nozzle; $\theta_{W,I} = 10.4^o$

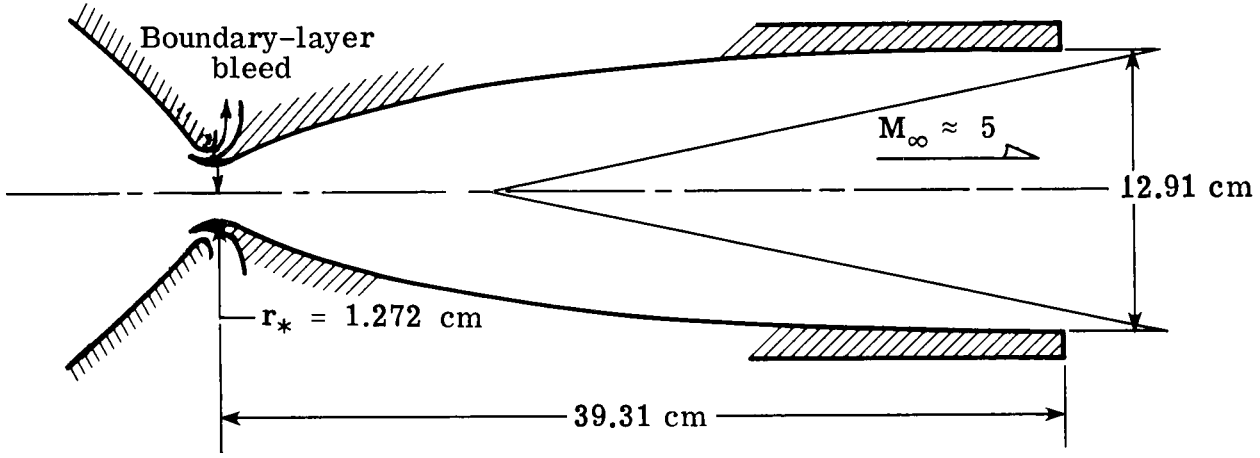

Slotted nozzle; $\theta_{W,I} = 22.6^o$

Figure 1.- Sketch of two Mach 5 axisymmetric nozzles.

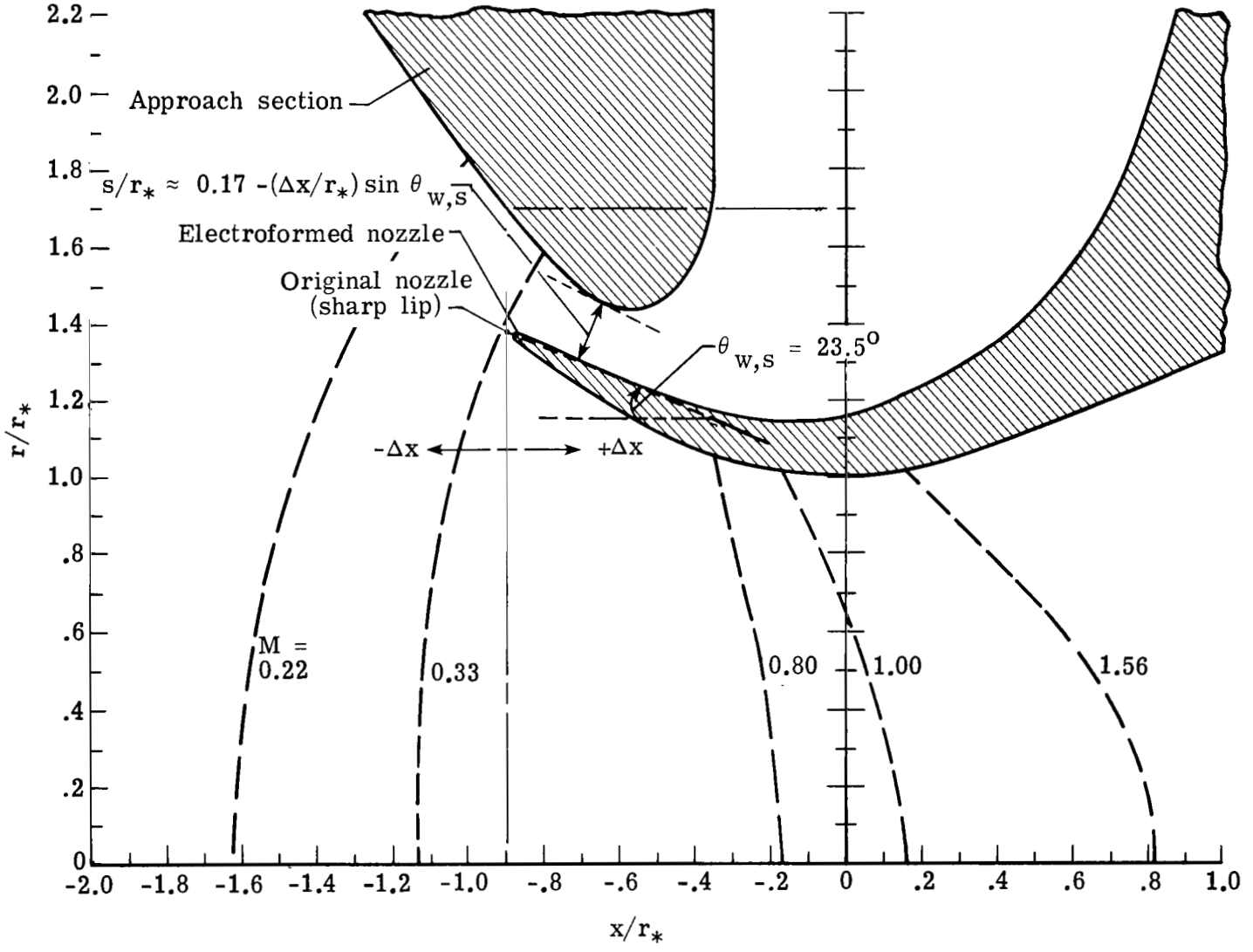

Figure 2.- Throat and slot region of slotted nozzle. Both electroformed and original nozzles shown in design position with respect to approach.

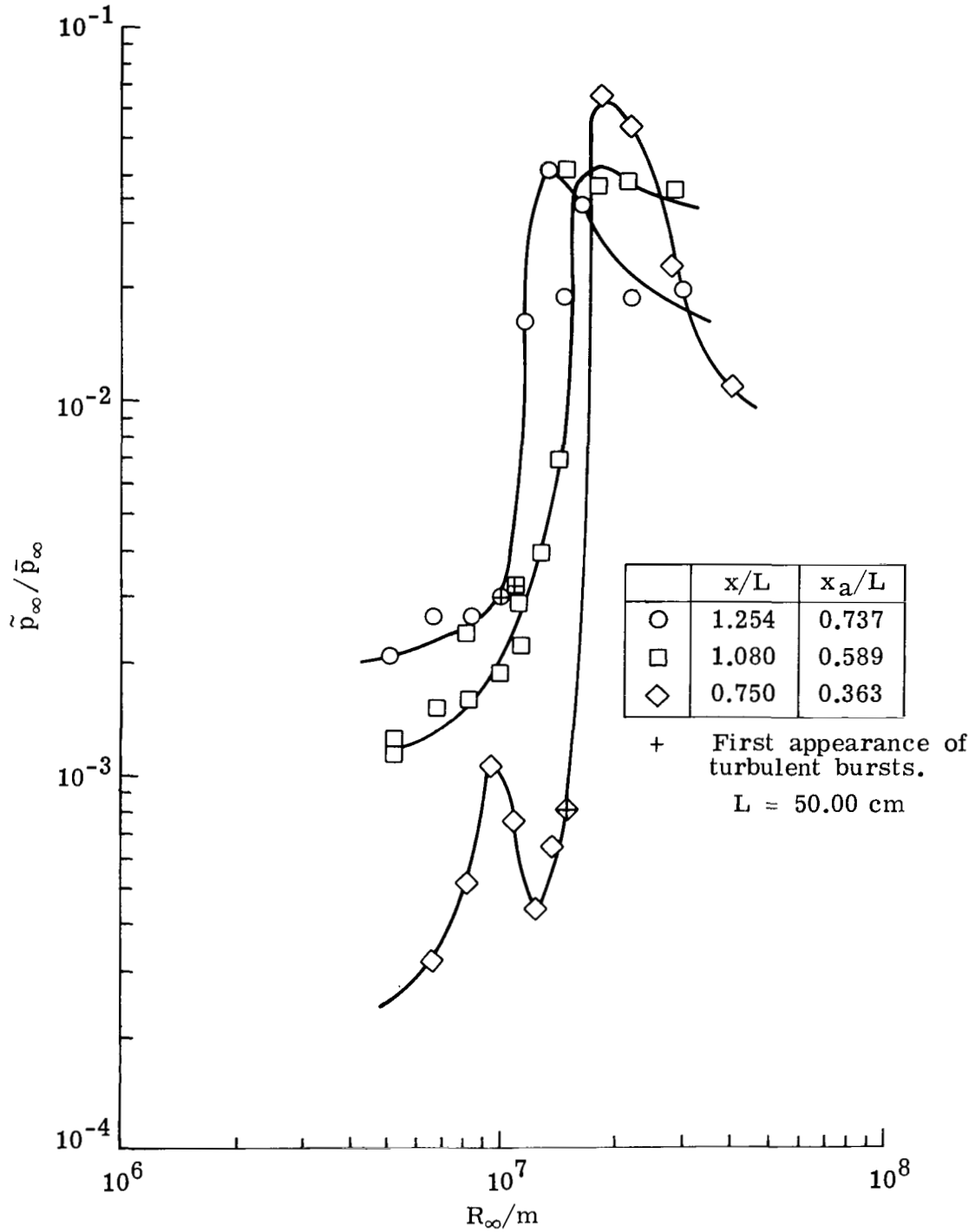

(a) Nozzle throat polished and maintained clean.

Figure 3.- Static-pressure fluctuations in conventional nozzle. From hot-wire data on center line (from ref. 13).

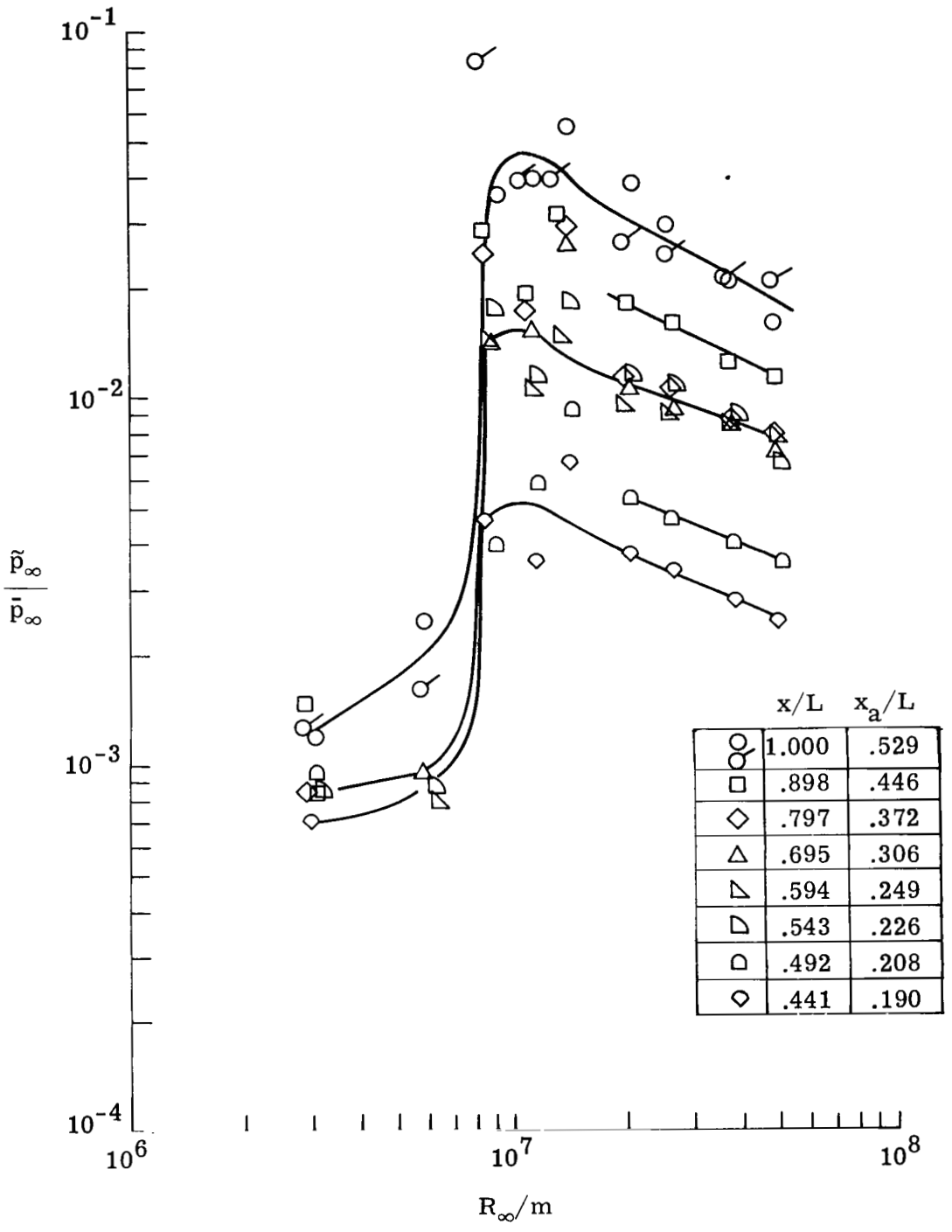

(b) Nozzle wall unpolished.

Figure 3.- Concluded.

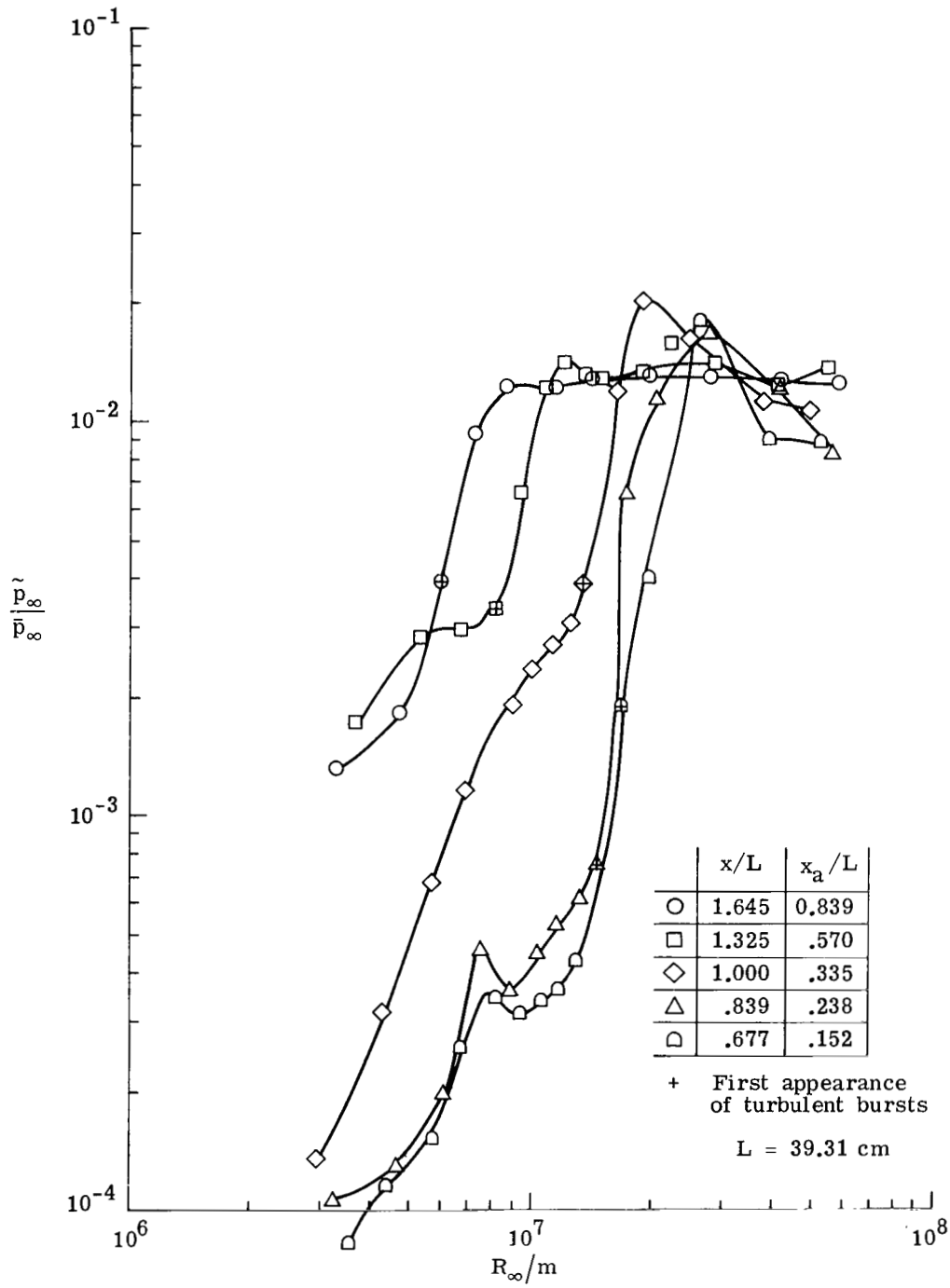

(a) From x = 26.6 cm to 64.7 cm.

Figure 4.- Static-pressure fluctuations in slotted nozzle with bleed valves open. From hot-wire data on center line.

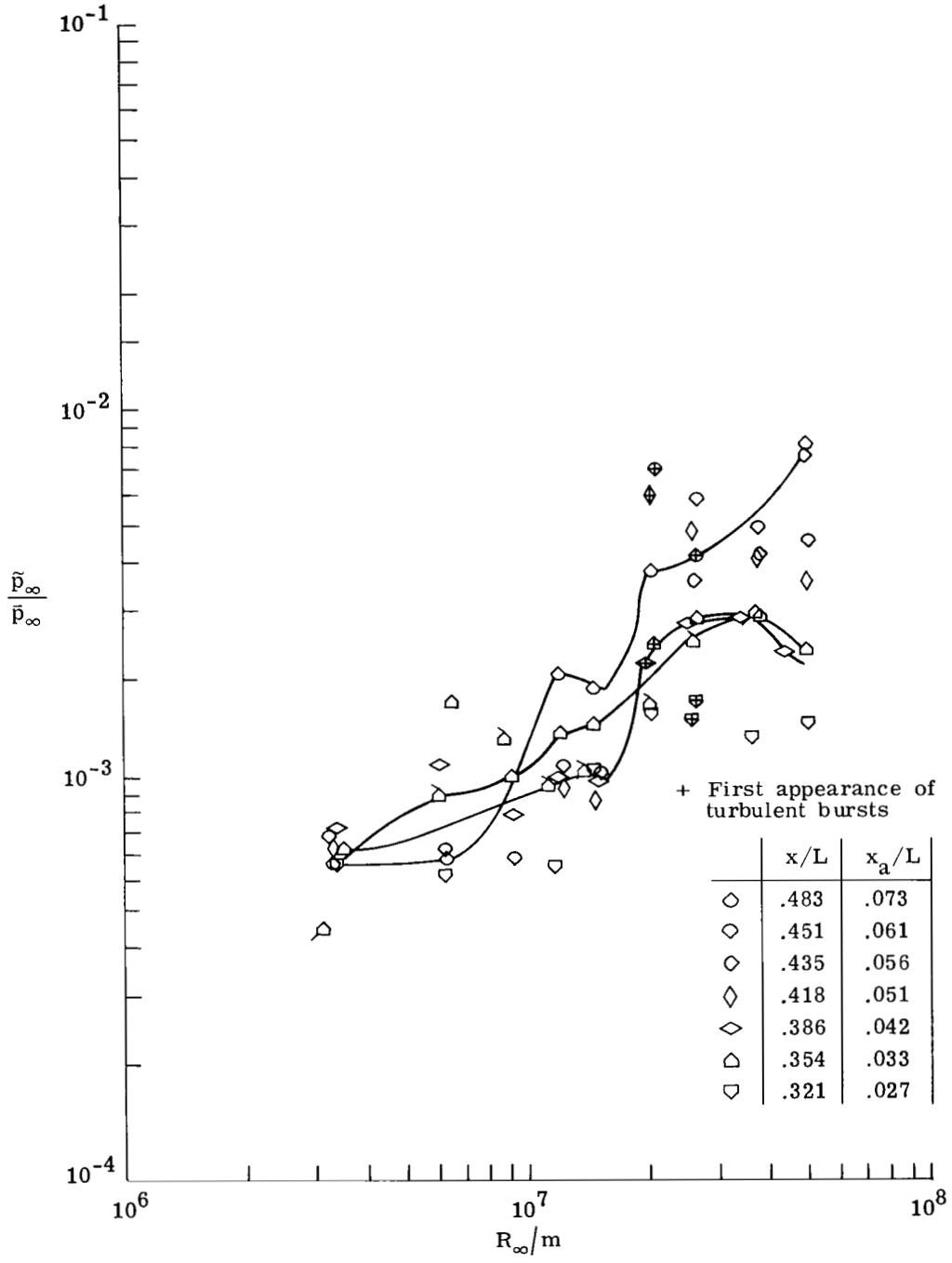

(b) From x = 12.6 cm to 19.0 cm; flagged symbols indicate repeat run.

Figure 4.- Concluded.

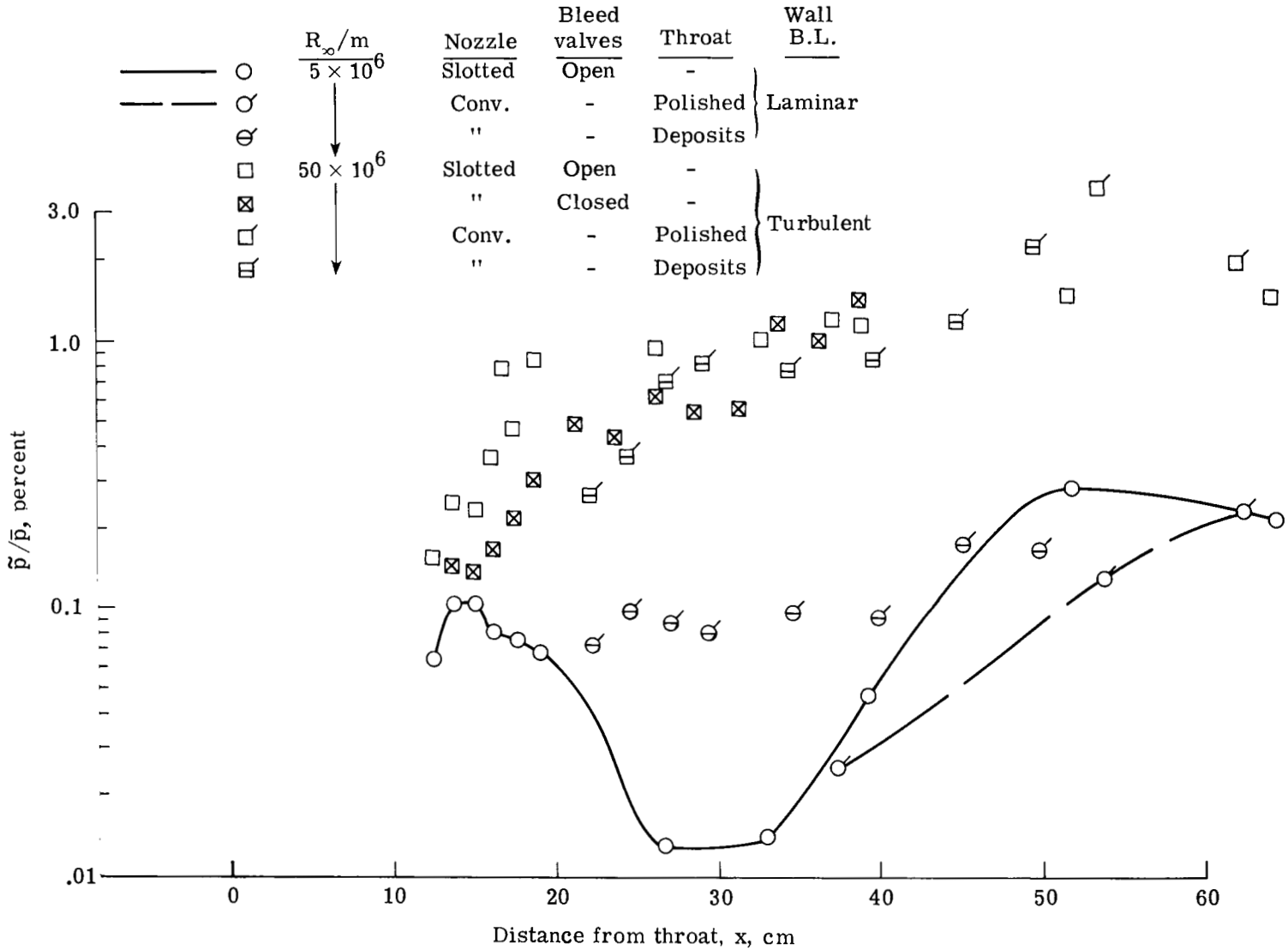

Figure 5.- Summary of rms static-pressure levels along center line of nozzles at two values of unit Reynolds number.

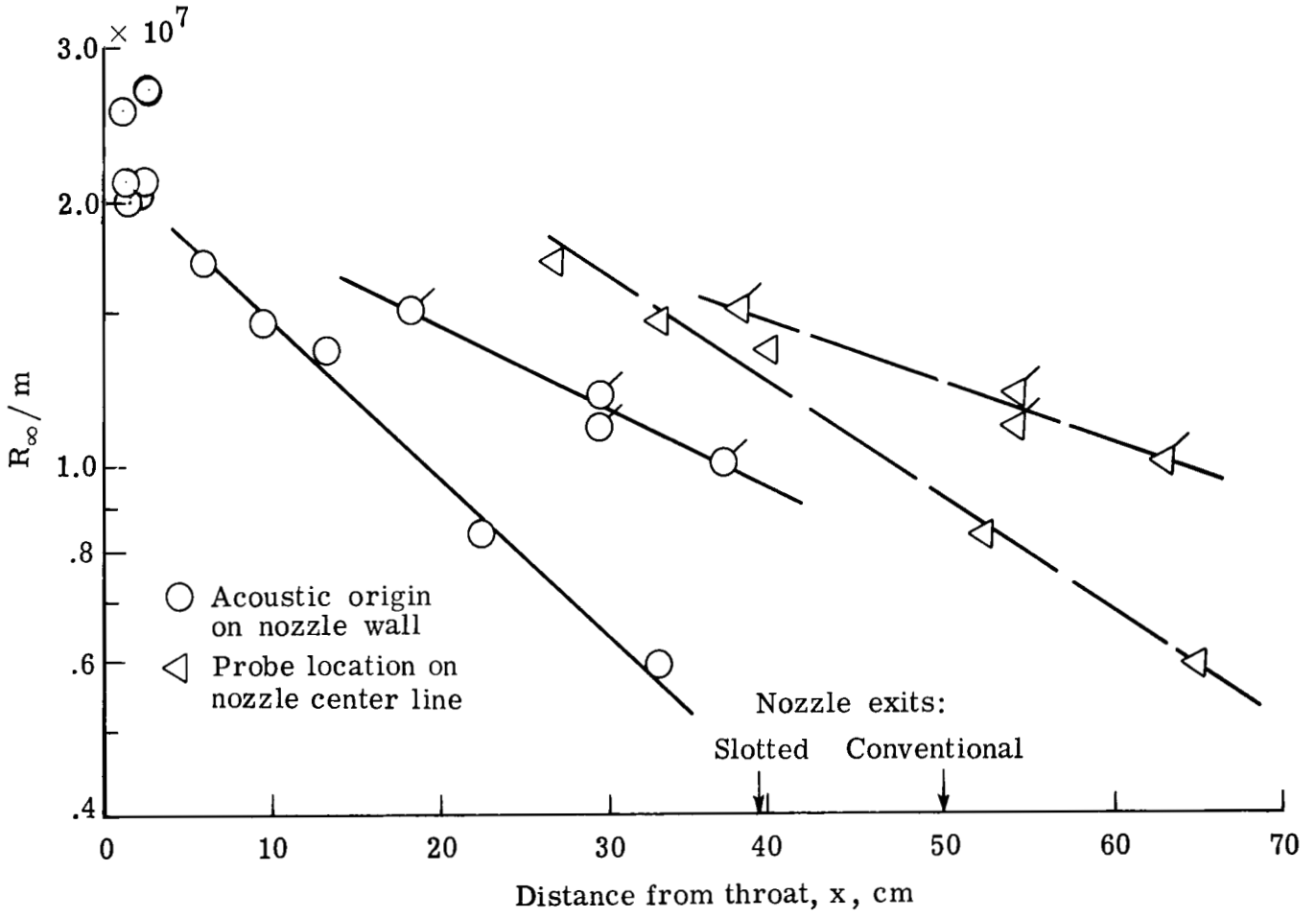

Figure 6.- Location of transition for several free-stream unit Reynolds numbers in nozzles. Flagged symbols are for conventional nozzle.

Nozzle entrance

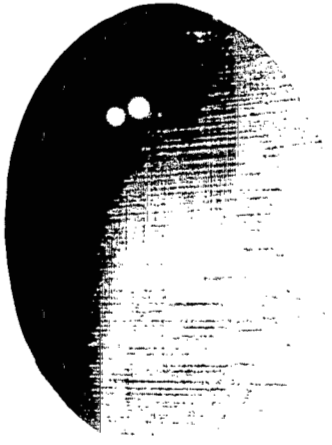

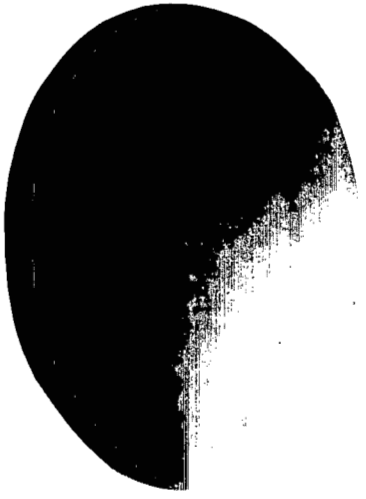

Nozzle exit

L-81-151

(a) $R_\infty = 5.6 \times 10^6/m$; laminar.

(b) $R_\infty = 1.2 \times 10^7/m$; turbulent.

Figure 7.- Oil flow streaks in conventional nozzle. Reference 12.

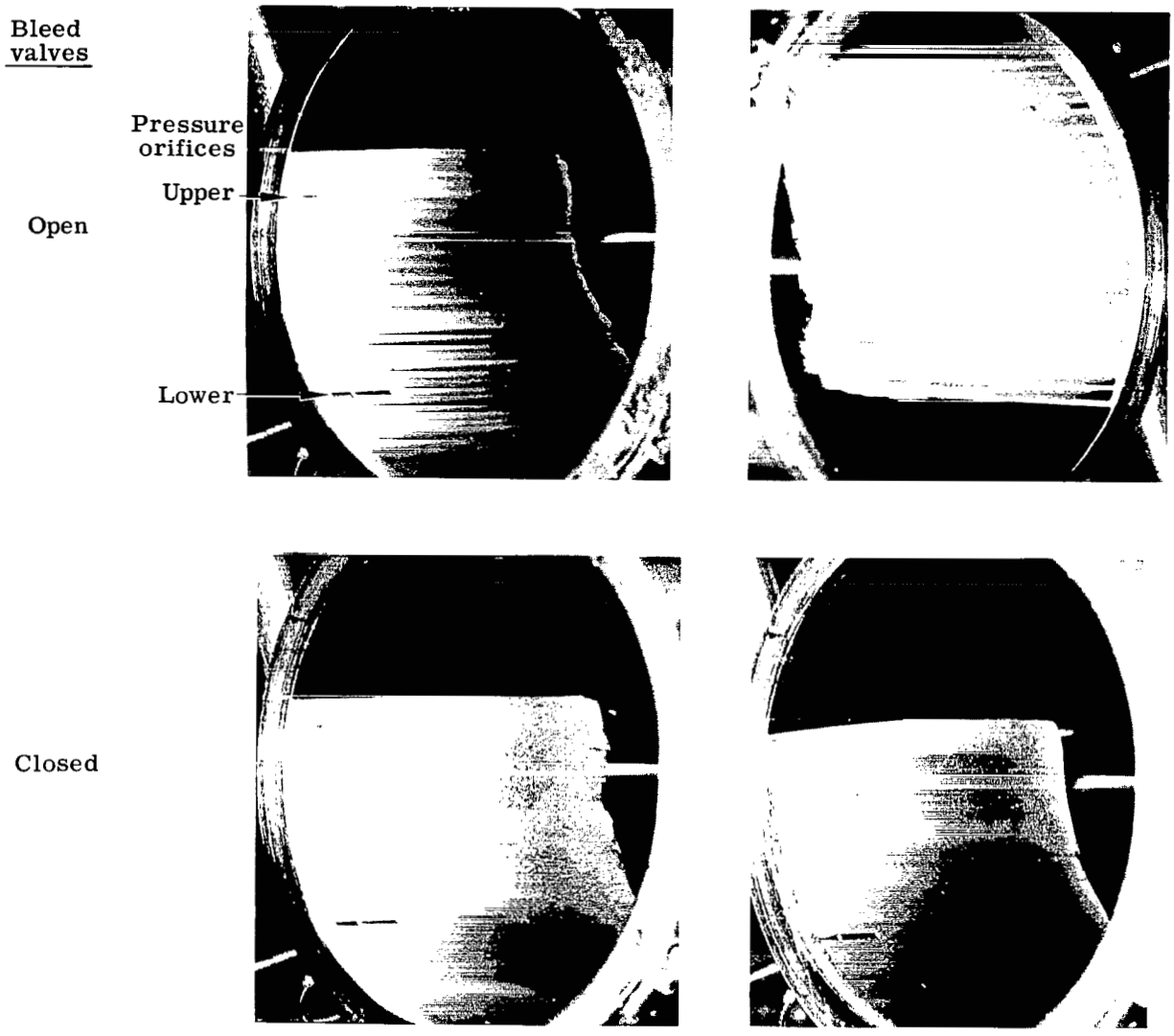

(a) $R_\infty \approx 0.5 \times 10^7/m.$ (b) $R_\infty \approx 0.9 \times 10^7/m.$

Figure 8.- Effect of unit Reynolds number and boundary-layer bleed on oil flow streaks near exit of slotted nozzle.

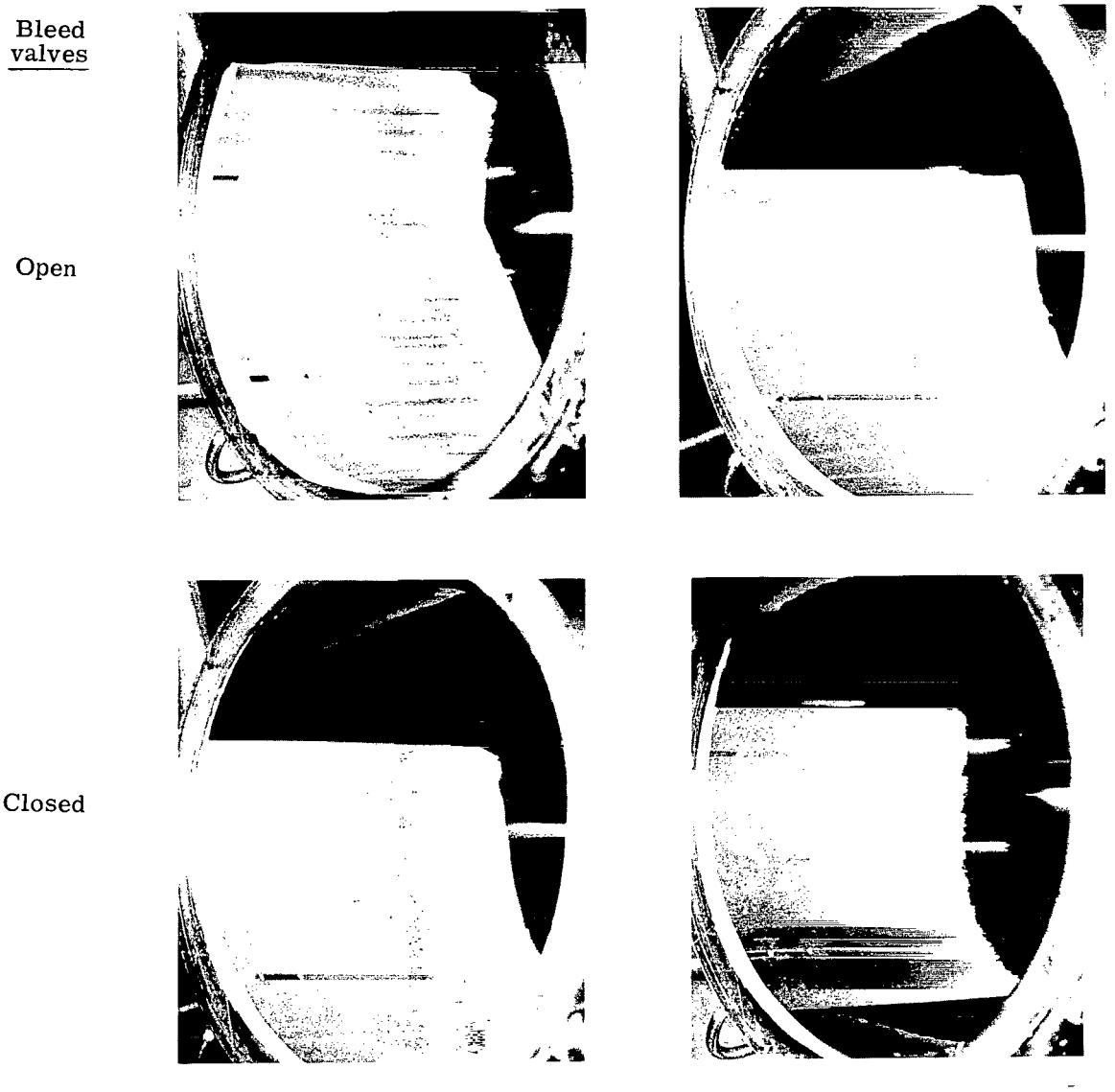

(c) $R_\infty \approx 1.4 \times 10^7/m.$

(d) $R_\infty \approx 2.7 \times 10^7/m.$

Figure 8.- Concluded.

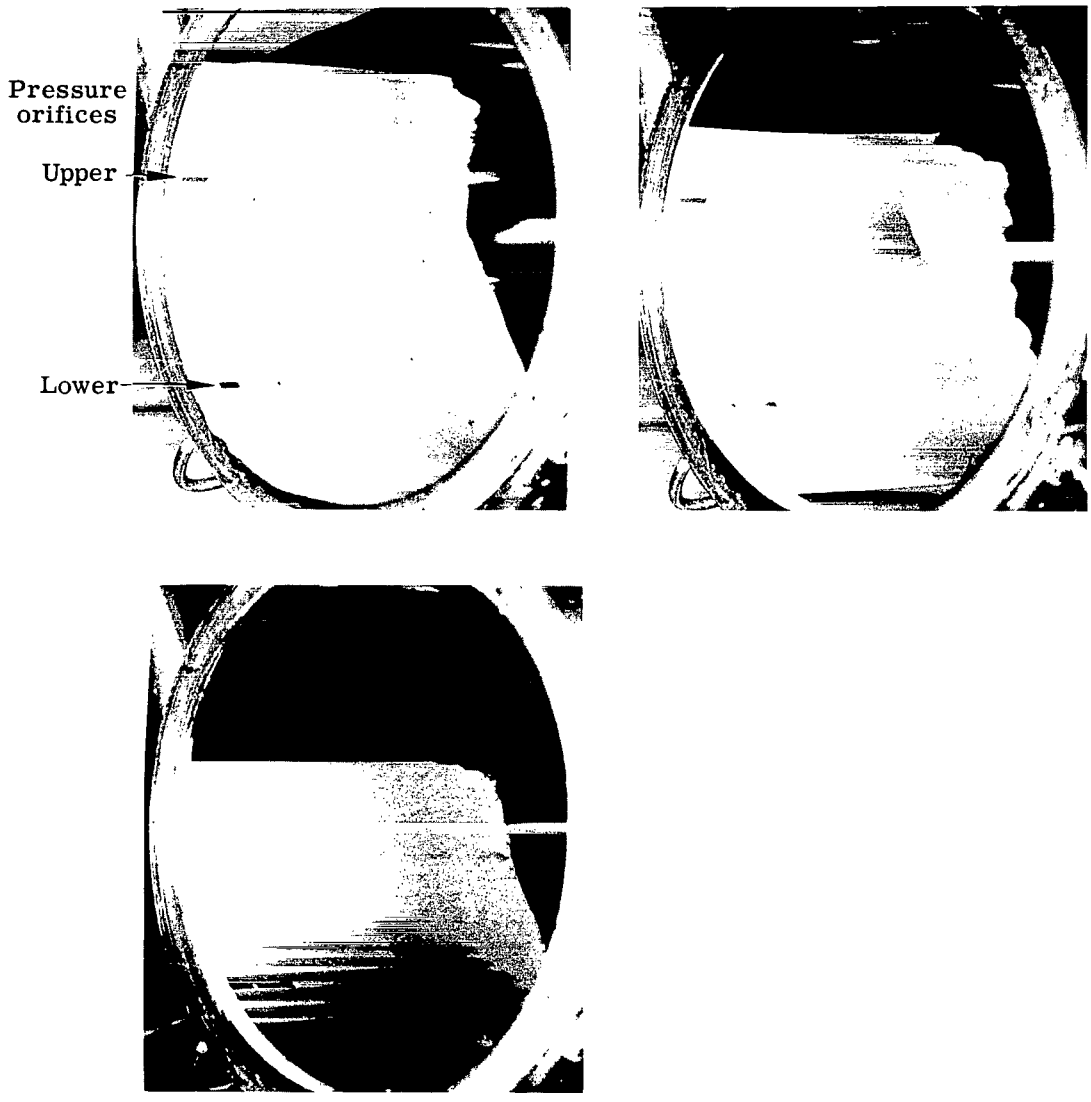

L-81-154

Figure 9.- Steady-state changes in oil streak patterns for different runs at $R_\infty \approx 1.4 \times 10^7/m$ in slotted nozzle with bleed valves open.

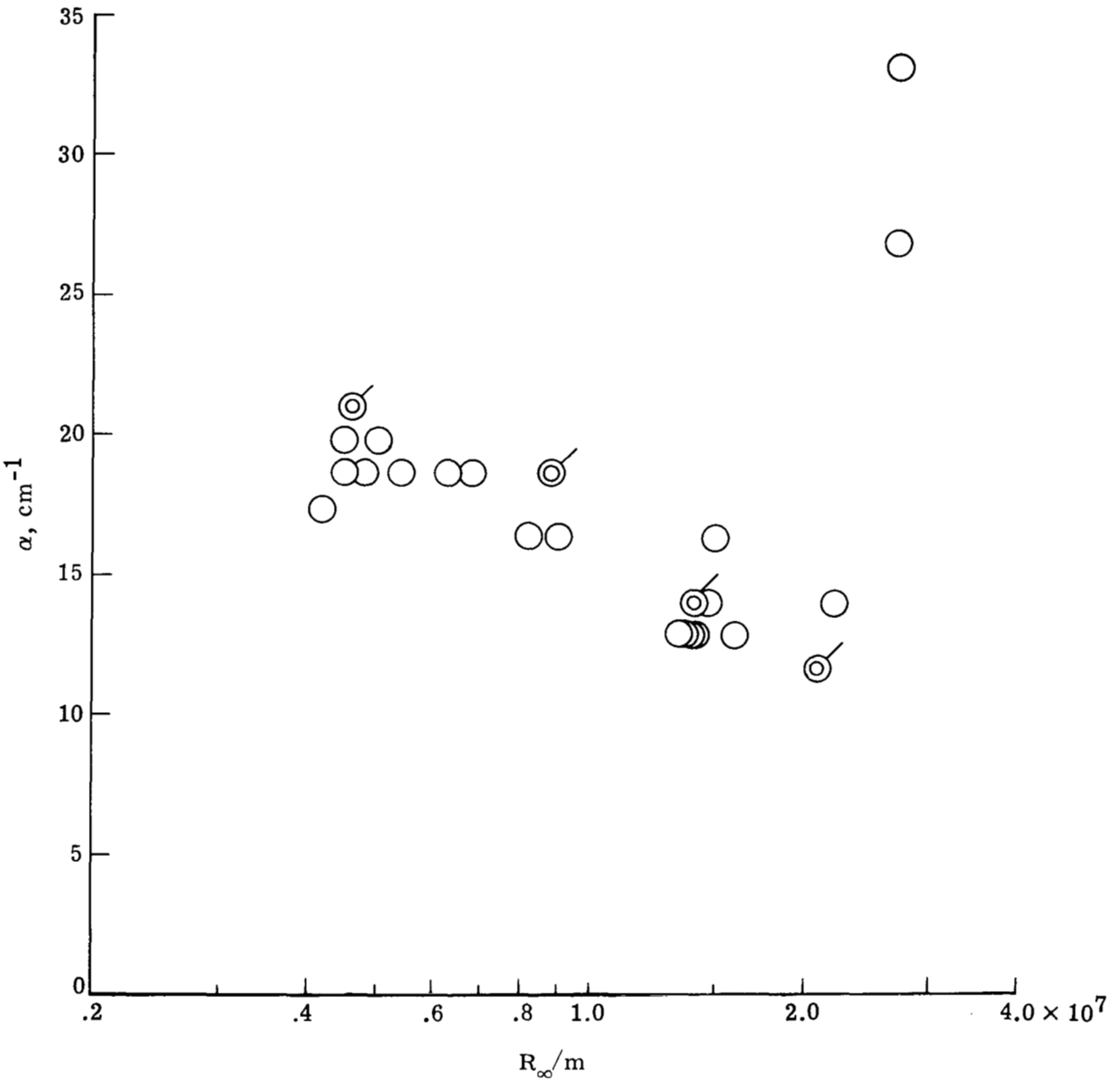

Figure 10.- Wave number of oil flow streaks near exit of slotted nozzle with bleed valves open. Values for flagged symbols used in figure 14.

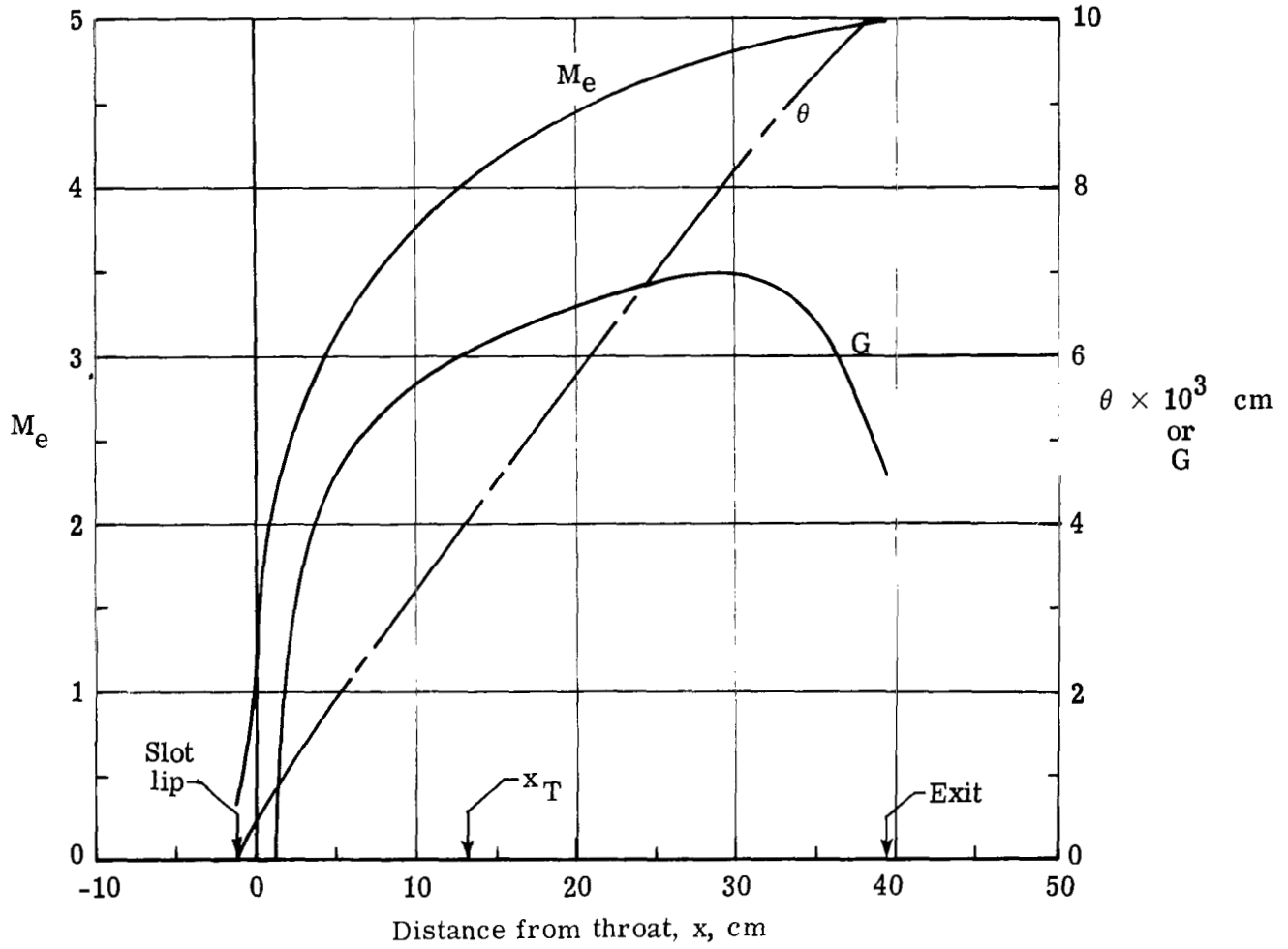

(a) Slotted nozzle; θ and G for $R_\infty = 1.35 \times 10^7/m$.

Figure 11.- Variation of M_e, θ, and G with axial distance from throat.

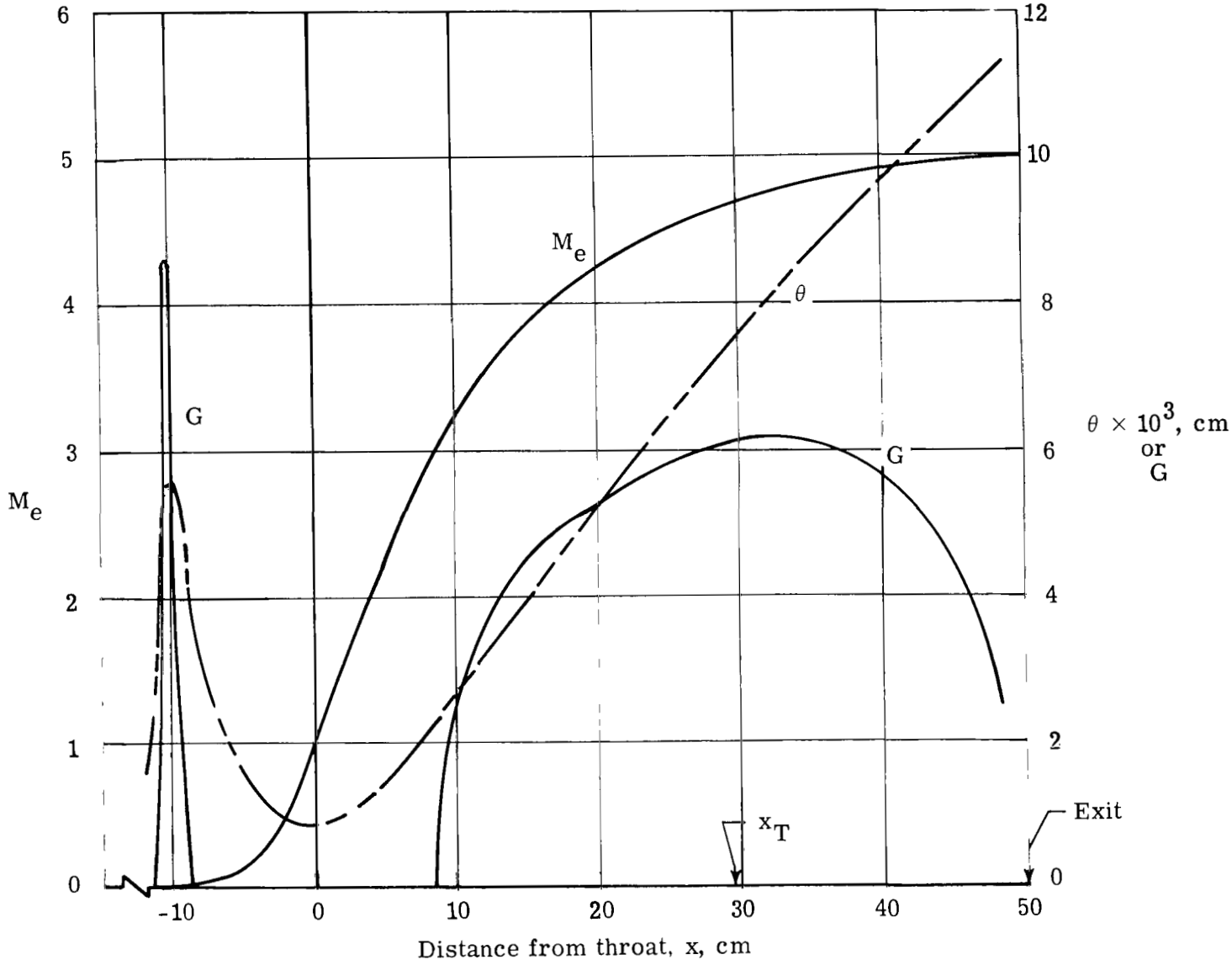

(b) Conventional nozzle; θ and G are for $R_\infty = 1.2 \times 10^7/m$.

Figure 11.- Concluded.

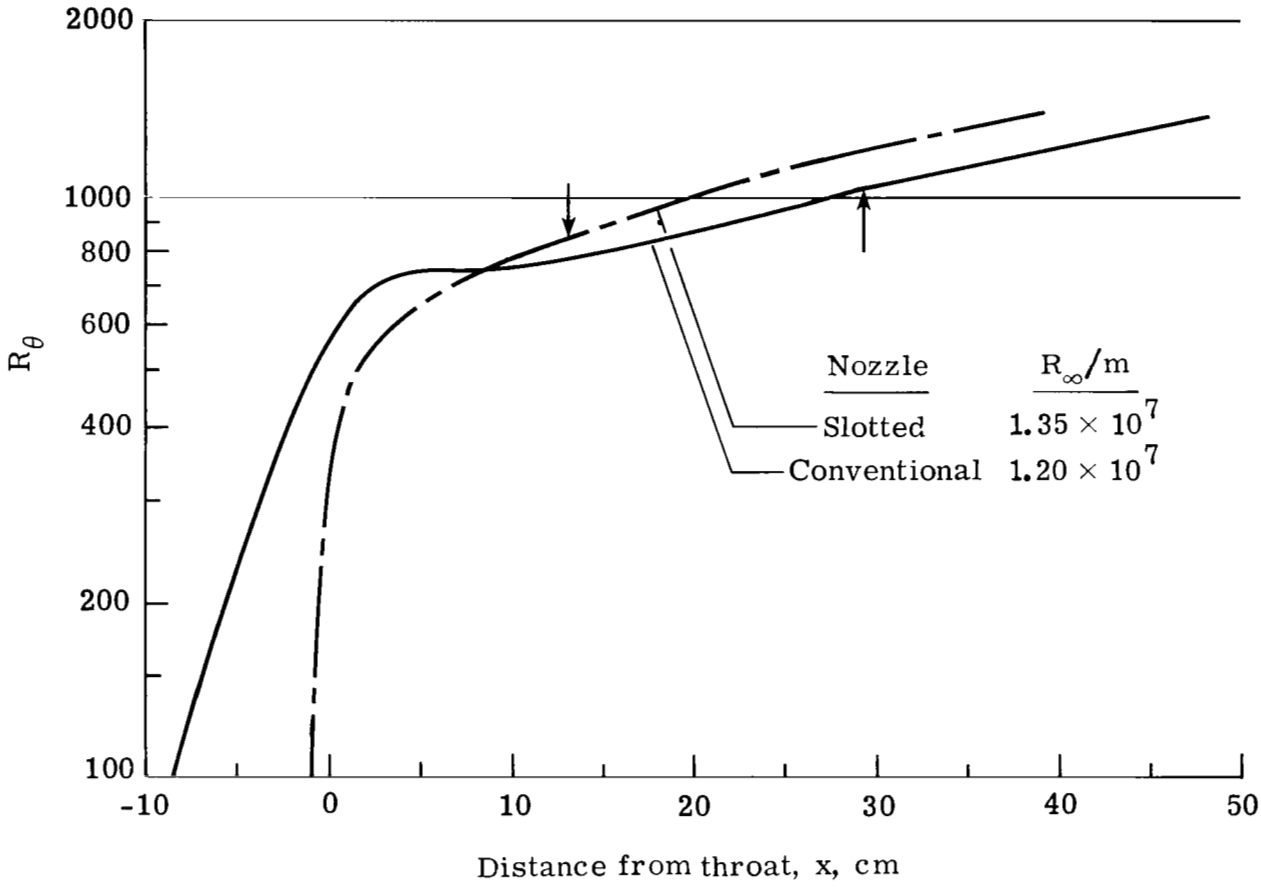

Figure 12.- Typical variations of momentum thickness Reynolds number for laminar boundary layer on wall of nozzles. Arrows indicate location of transition at given values of R_∞.

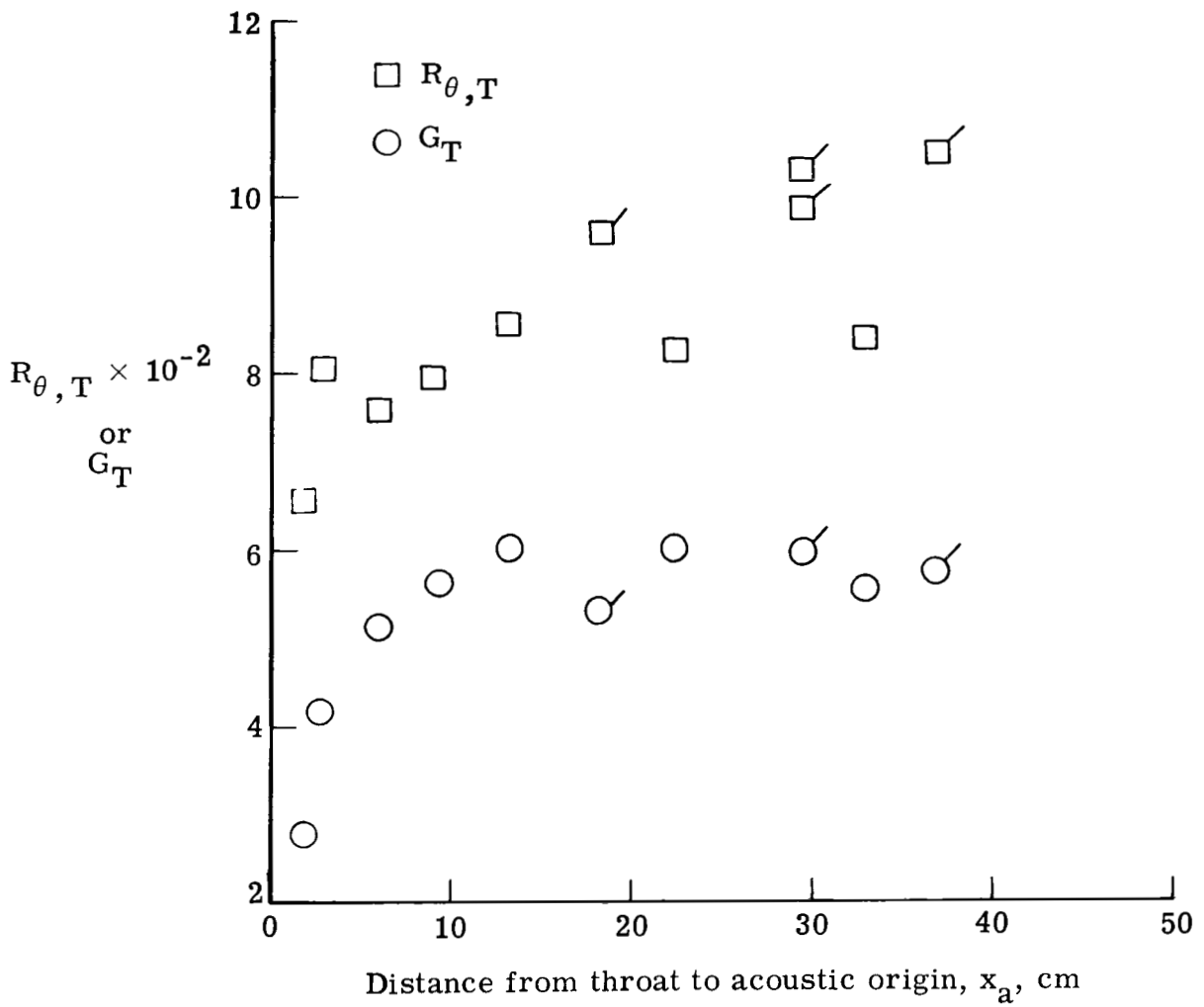

Figure 13.- Local momentum thickness Reynolds number and Görtler number at transition on nozzle walls. Flagged symbols indicate conventional nozzle.

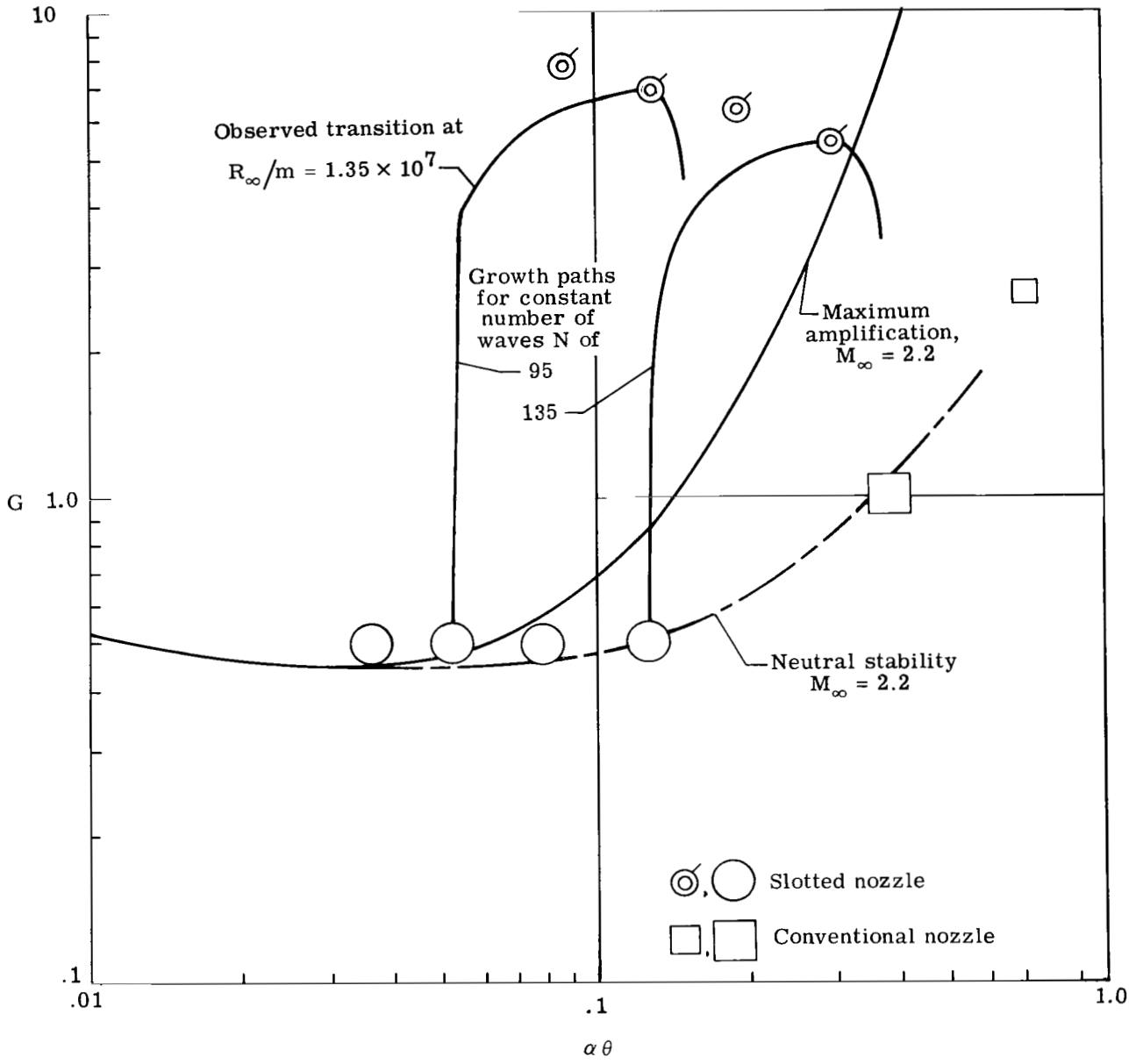

Figure 14.- Variation of Görtler number with wave number. Small symbols use α from observed oil streaks; large symbols at $G \approx 0.5$ and 1.0 for slotted and conventional nozzle, respectively, utilize laminar boundary-layer conditions at approximate upstream location of instability onset assuming constant N.

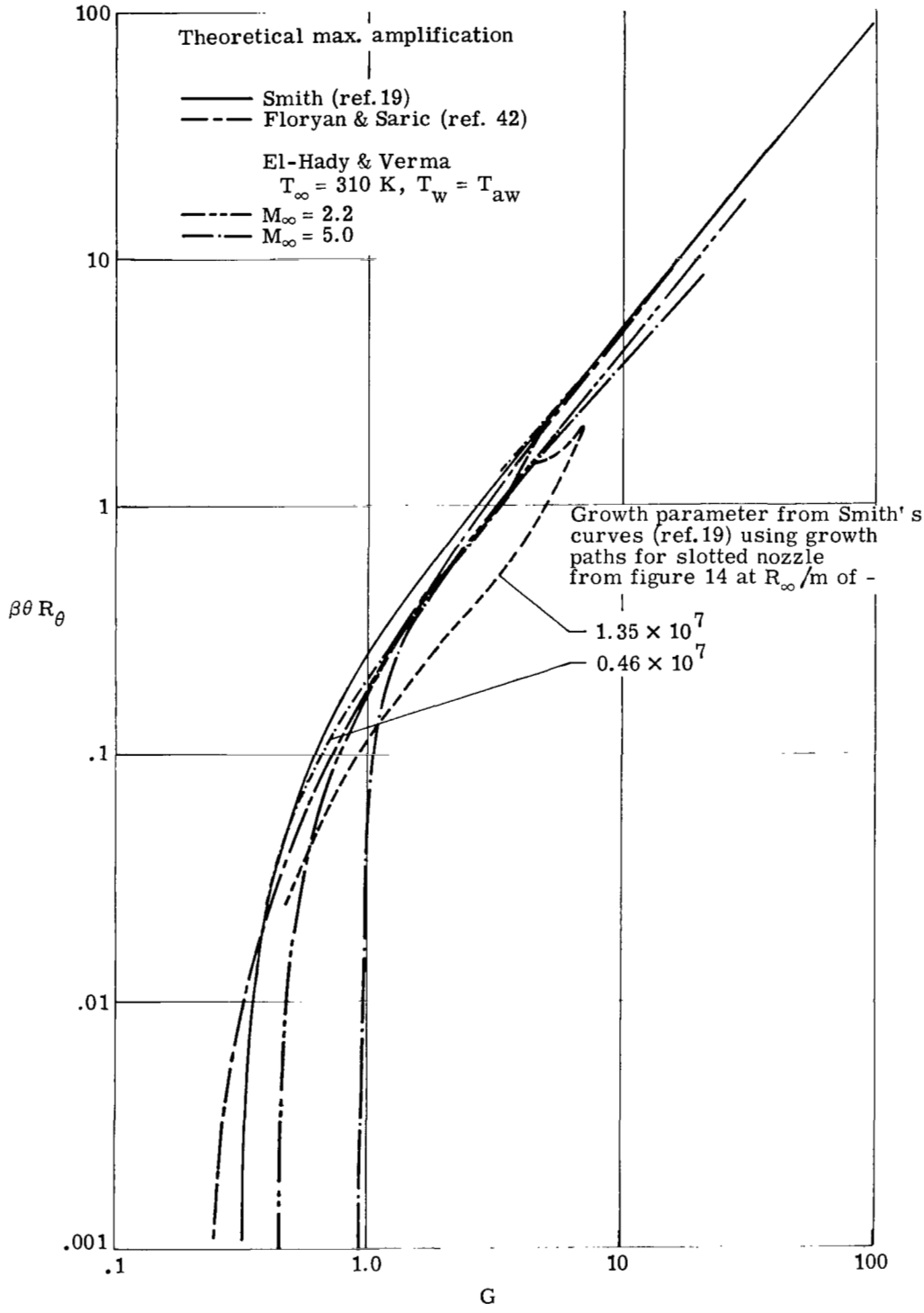

Figure 15.- Variation of normalized growth parameter with Görtler number.

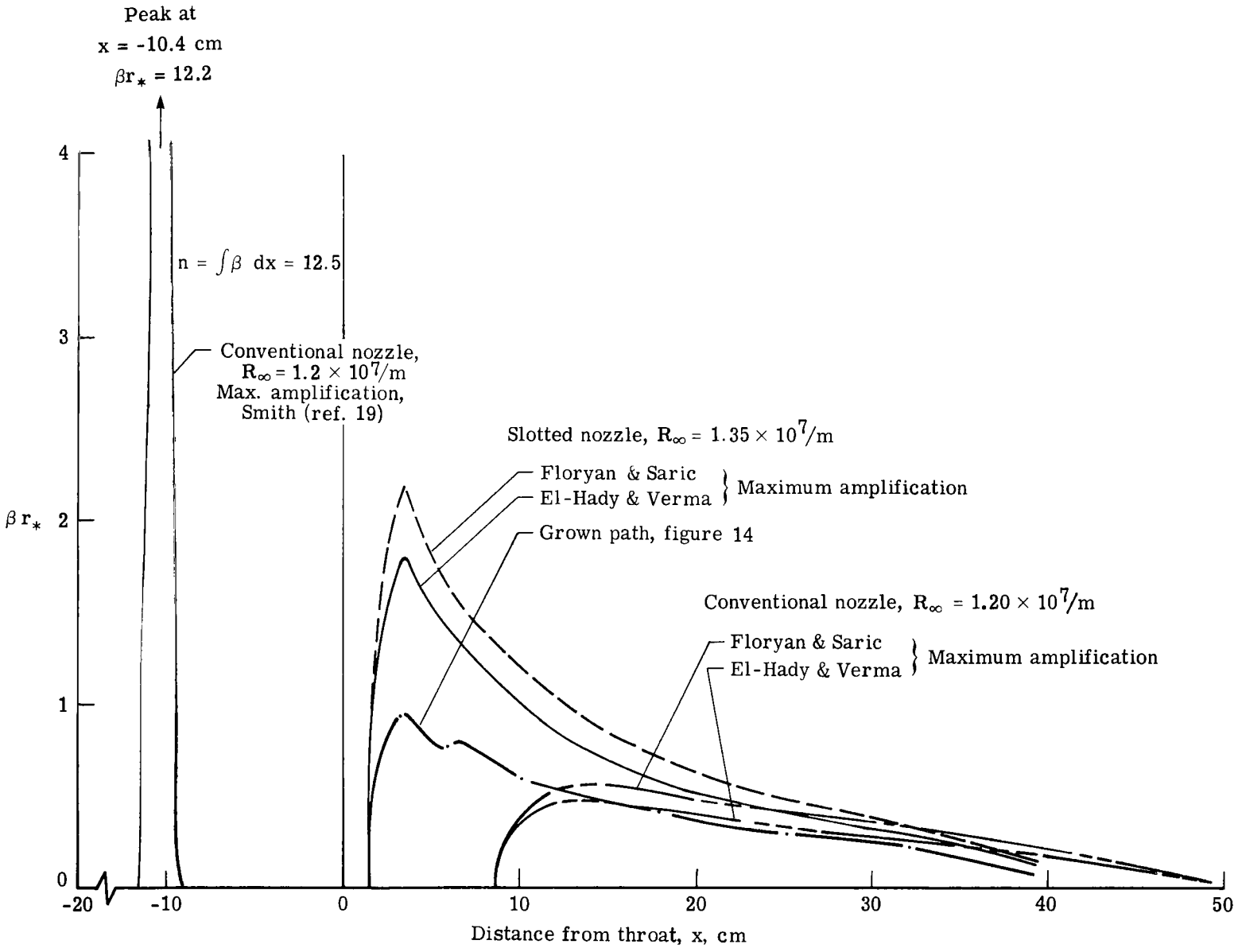

Figure 16.- Typical variations of local amplification rate factor in nozzles.

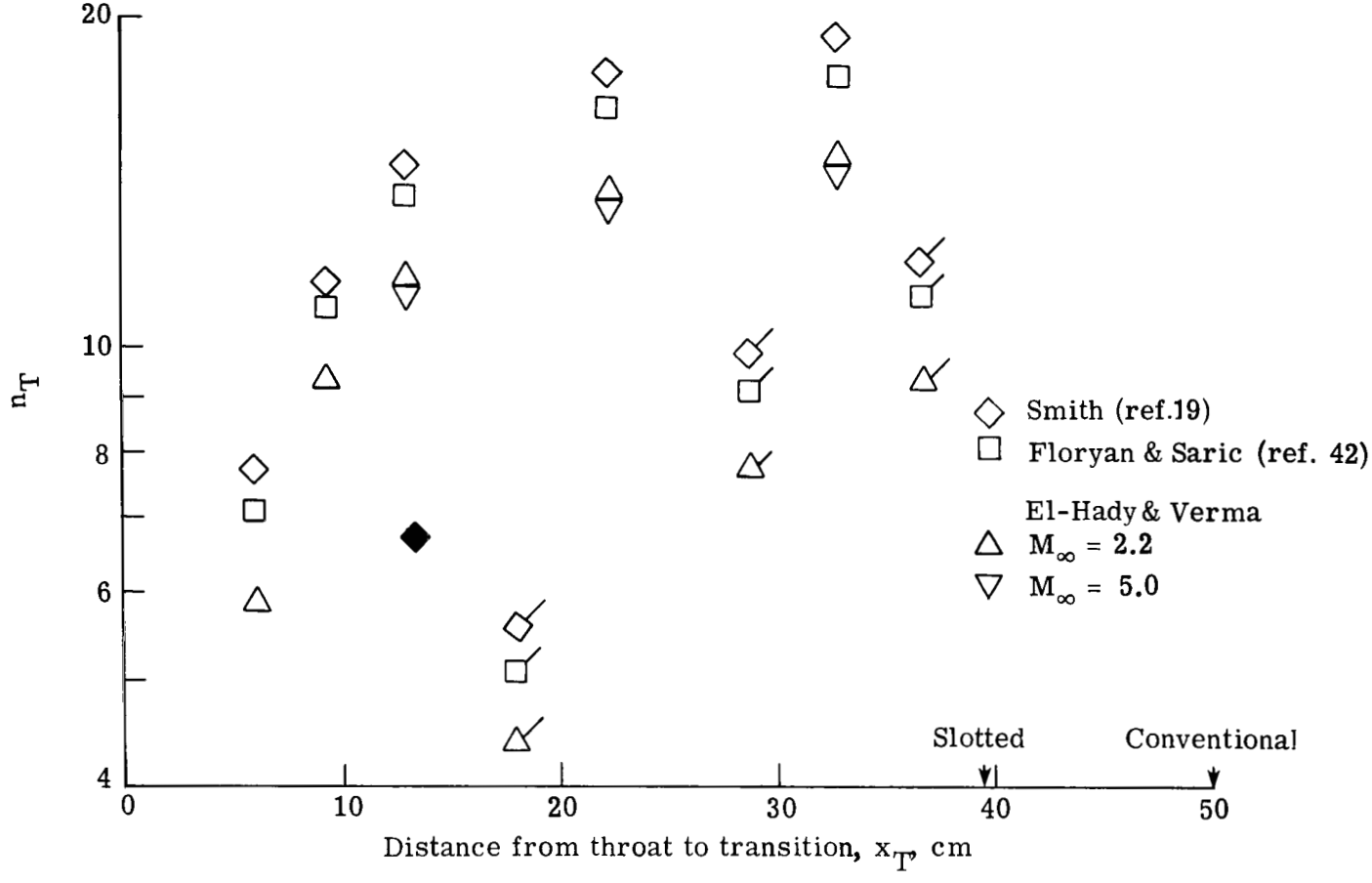

Figure 17.- Integrated growth factor $n_T = \int_{x_{\beta=0}}^{x_T} \beta \, dx$ to transition in nozzles.

Arrows indicate location of nozzle exits. Flagged symbols indicate conventional nozzle; solid symbol indicates growth path from figure 15.

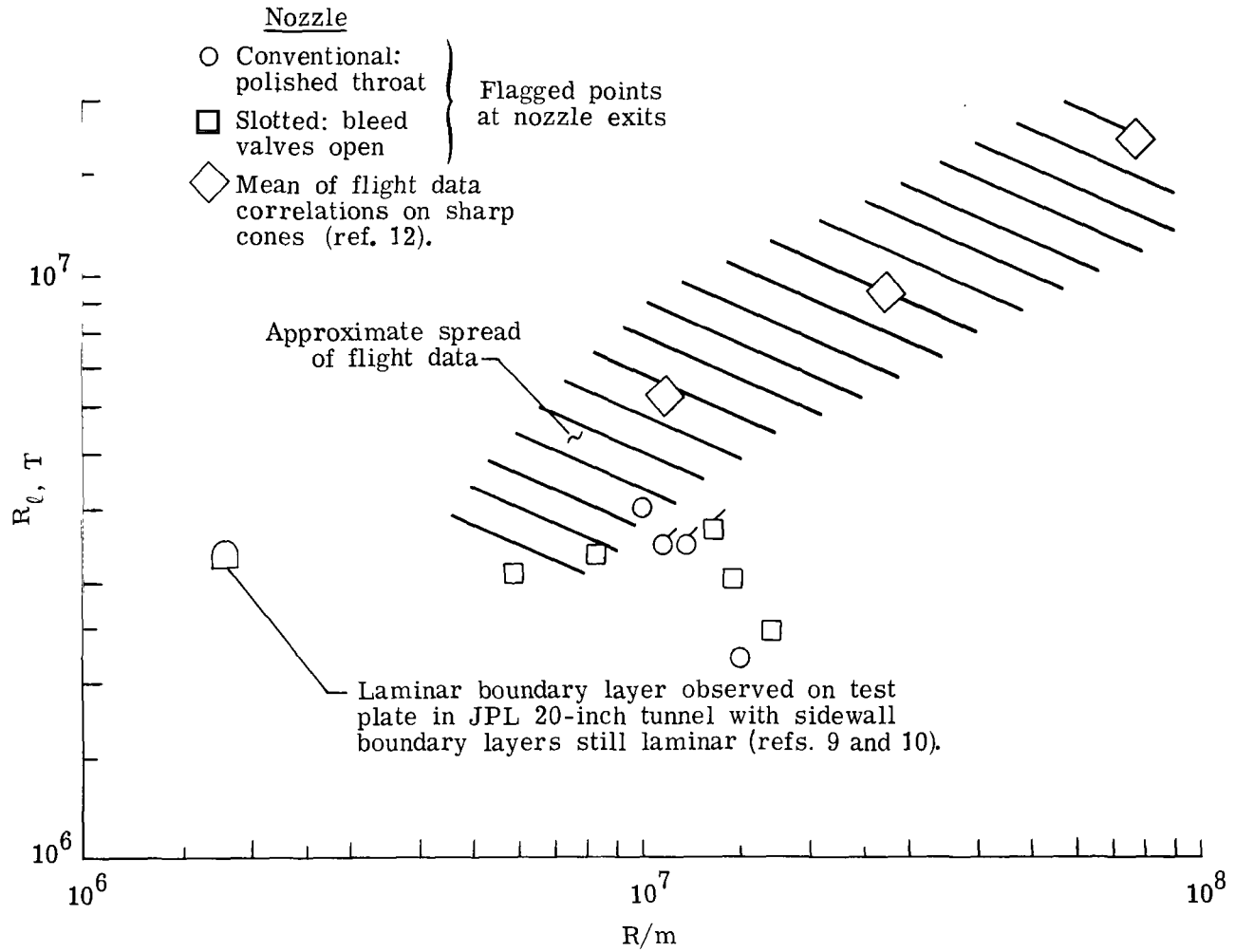

Figure 18.- Transition Reynolds number variation with unit Reynolds number. For nozzle data, ℓ is test rhombus length along center line exposed to noise radiation from laminar wall boundary layers; for cone data, ℓ is wetted length from the cone tip to onset of transition.

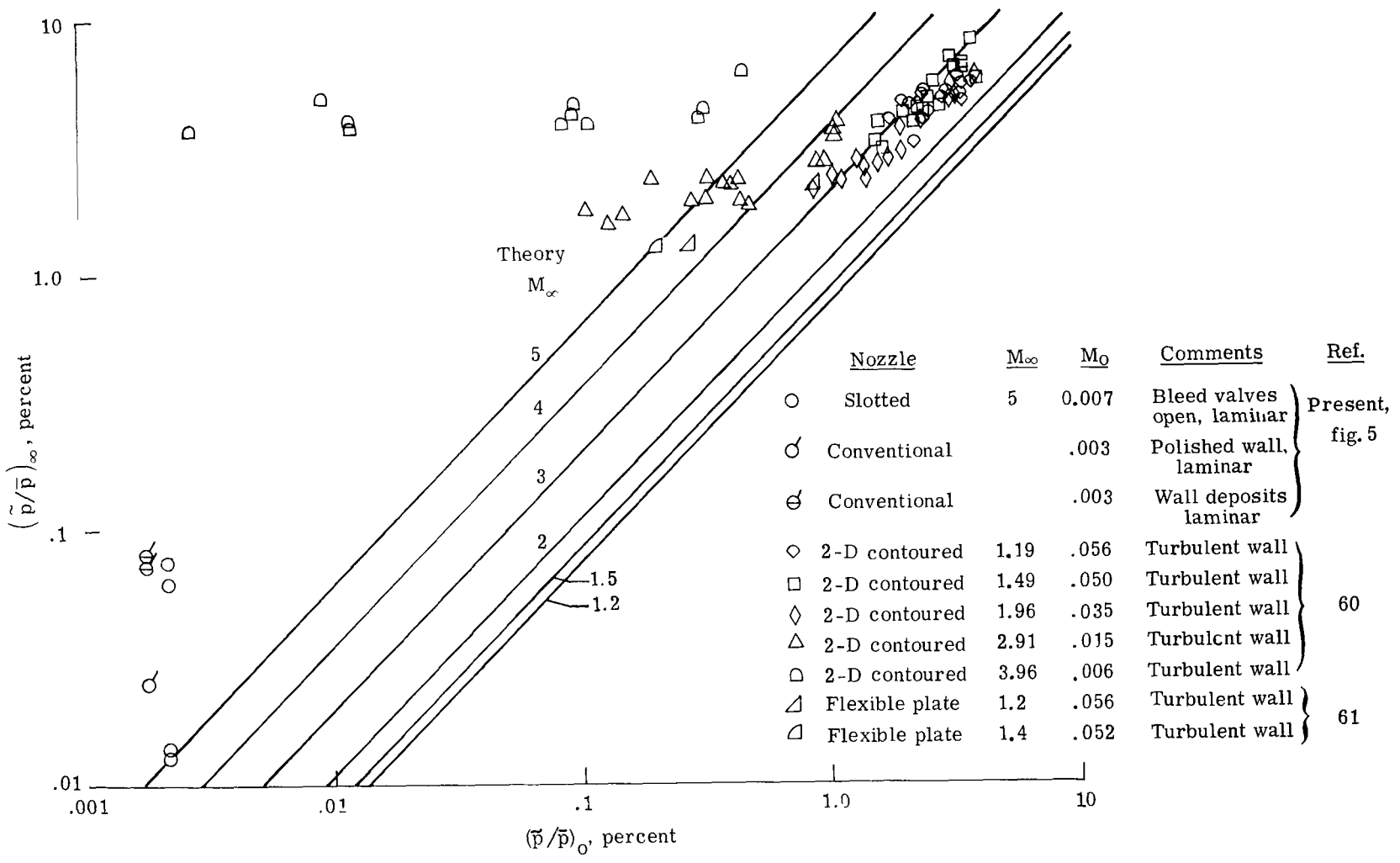

(a) Comparison of experimental data with constant area ray-tube theory, equation (A7), K = 1.0.

Figure 19.- Dependence of test section noise levels on settling chamber noise levels.

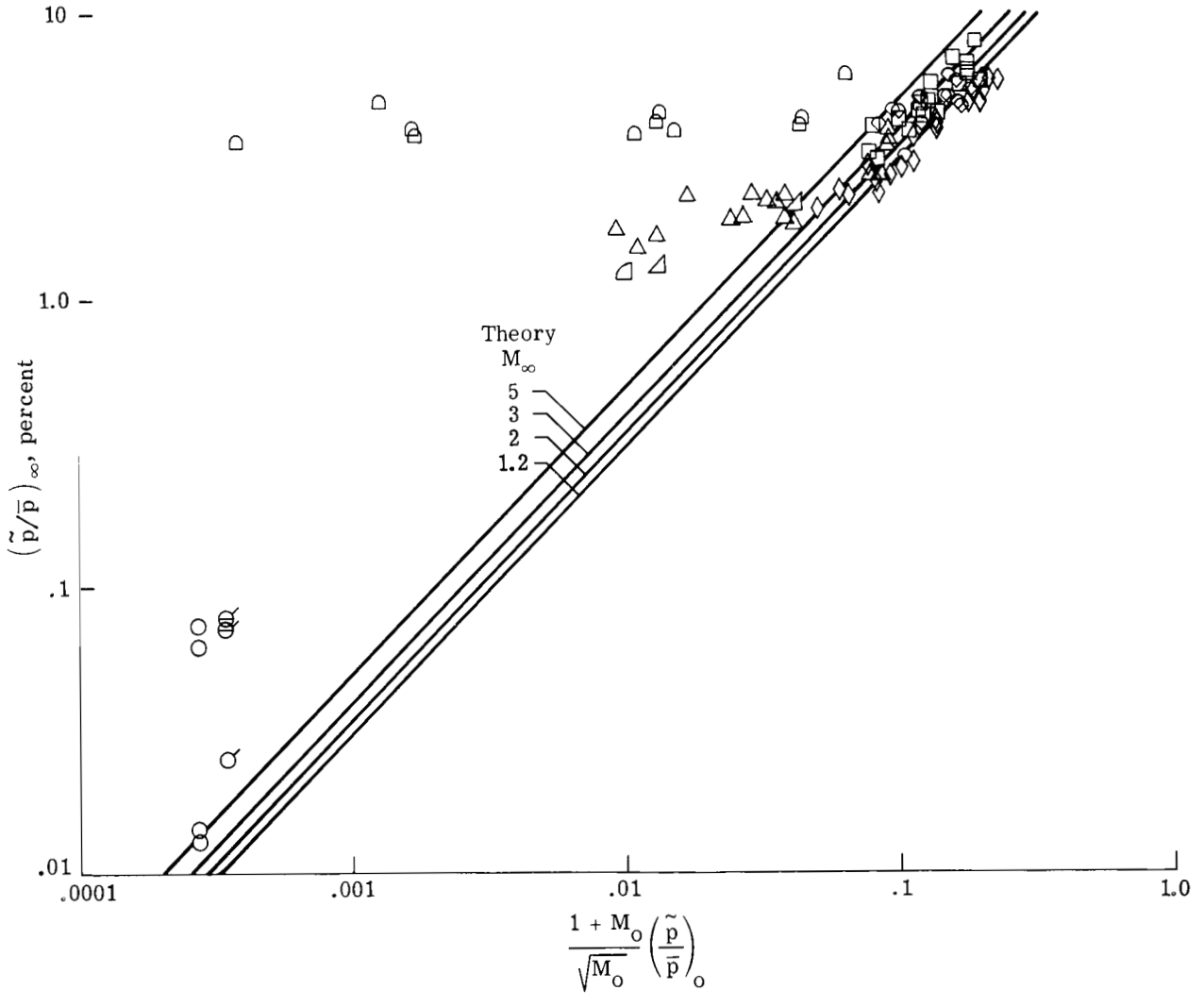

(b) Comparison of experimental data with Candel's theory (ref. 58), equation (A6), K = 0.3.

Figure 19.- Concluded.

1. Report No.	2. Government Accession No.	3. Recipient's Catalog No.
NASA TP-1869		

4. Title and Subtitle	5. Report Date
GÖRTLER VORTICES AND TRANSITION IN WALL BOUNDARY LAYERS OF TWO MACH 5 NOZZLES	August 1981
	6. Performing Organization Code 505-31-23-04
7. Author(s)	8. Performing Organization Report No.
Ivan E. Beckwith and Barbara B. Holley	L-14332
	10. Work Unit No.
9. Performing Organization Name and Address	
NASA Langley Research Center Hampton, VA 23665	11. Contract or Grant No.
	13. Type of Report and Period Covered
12. Sponsoring Agency Name and Address	Technical Paper
National Aeronautics and Space Administration Washington, DC 20546	14. Sponsoring Agency Code

15. Supplementary Notes

16. Abstract

The onset of transition in the wall boundary layers of two axisymmetric Mach 5 wind-tunnel nozzles has been measured under conditions of extremely low incident disturbance levels. The range of test unit Reynolds numbers, based on conditions at the nozzle exit, was from 6×10^6/m to 2.5×10^7/m. When the nozzle walls were maintained in a polished and clean condition, transition moved gradually upstream as the test Reynolds number was increased. When transition occurred in the supersonic concave wall region, the values of the local Görtler parameter at transition varied from about 5 to 6, whereas the momentum thickness Reynolds number varied from about 750 to 1050. Oil flow patterns obtained near the exit of the nozzles indicated that Görtler vortices were always present when the wall boundary layers were laminar. Calculations for the growth of Görtler vortices based on new results from linear theory for supersonic flat-plate profiles gave amplification ratios to transition from e^4 to e^{15}. Possible reasons for this wide range in amplification ratios are discussed, but no definite conclusions are yet possible regarding the values of n in a simple e^n type theory for the assumed linear amplification of Görtler vortices to transition in supersonic nozzles.

17. Key Words (Suggested by Author(s))	18. Distribution Statement
Supersonic wind tunnel Boundary layer Görtler vortices Transition Free-stream noise	Unclassified - Unlimited Subject Category 34

19. Security Classif. (of this report)	20. Security Classif. (of this page)	21. No. of Pages	22. Price
Unclassified	Unclassified	70	A04

For sale by the National Technical Information Service, Springfield, Virginia 22161

NASA-Langley, 1981

National Aeronautics and
Space Administration

Washington, D.C.
20546

Official Business
Penalty for Private Use, $300

THIRD-CLASS BULK RATE

Postage and Fees Paid
National Aeronautics and
Space Administration
NASA-451

U.S.MAIL

8 1 1U,D, 082181 S00903DS
DEPT OF THE AIR FORCE
AF WEAPONS LABORATORY
ATTN: TECHNICAL LIBRARY (SUL)
KIRTLAND AFB NM 87117

NASA

POSTMASTER: If Undeliverable (Section 158 Postal Manual) Do Not Return